2010 Human Powered Vehicle Challenge West
Sponsored by ASME and California State University, Northridge (CSUN)

Form 6: Vehicle Description
Due March 22, 2010

(Dimensions in inches, pounds)

Competition Location: Northridge, California

School name: Rose-Hulman Institute of Technology

Vehicle name: Ragnarök

Vehicle number 1

Vehicle type Unrestricted X Speed_____

Vehicle configuration

Upright _____ Semi-recumbent _____

Prone _____ Other (specify) Recumbent Interchangeable Tilting Trike

Frame material carbon fiber and aramid

Fairing material(s) carbon fiber and aramid

Number of wheels 2 (or 3)

Vehicle Dimensions

Length 93 in Width 29.5 in (in three wheel mode)

Height 40 in Wheelbase 45.3 in

Weight Distribution Front 40% Rear 60% Total 100%

Wheel Size Front ISO406 Rear ISO406

Frontal area 585 in^2

Steering Front X Rear _____

Braking Front _____ Rear _____ Both X

Estimated Cd 0.067

Vehicle history (e.g., has it competed before? where? when?)

_____

_____

_____

_____

_____

Rose-Hulman Institute of Technology

2010 ASME East Coast HPV Challenge

Unrestricted Class Entry

Presents

Team Officers

Jeffery Van Treuren
Christopher Wlezien
Ariel Young
Jeffrey Dovalovsky

Team Members

Andrew Bomar
Andrew Boneff
Rachelle Cobb
Sean Hannon
Edward Mayhew
Cole Pearson
Ethan Rockett
Petras Swissler
Jeremy Webb

For more team information visit the team website at:
www.rose-hulman.edu/hpv

Contents

1 Abstract

For 2010, the Rose-Hulman Human Powered Vehicles Team (HPVT) will be competing in the new unrestricted class in the Human-Powered Vehicle Challenge (HPVC) sponsored by the American Society of Mechanical Engineers (AMSE). Early on, the HPVT defined a mission statement for the 2010 competition year:

> The Rose-Hulman HPVT will be competing in the ASME 2010 HPVC Unrestricted Class. In order to meet the challenges of this competition the team will focus their design on the new goals of practicality and versatility while keeping their previous goals of durability, speed, and safety a high priority. A combination of innovation and tradition is integral to future success and it is the Rose-Hulman HPVT's mission to Design, Test, Build, and Race their new vehicle, Ragnarök, by using all available resources and experience to achieve their design goals.

The HPVT has kept to this mission while designing and building the 2010 vehicle, the Ragnarök. The intended user of a vehicle in the old "utility" class is a commuter. The new unrestricted class combines the features necessary for a commuter with the speed capabilities of a vehicle designed for human-powered vehicle (HPV) racing. The HPVT has developed many new features to meet the functionality requirements of this new vehicle class, most notably a tilting trike mechanism that can be interchanged with a standard rear wheel. Extensive analysis was performed to develop this mechanism, along with a prototype to optimize the function of the device (Figure 1). Most of the functionality features, including the tilting trike, were developed to be removable to allow the vehicle to be outfitted for racing. Various forms of aerodynamic testing were performed to develop the Ragnarök's speed capabilities. Structural analysis and testing were performed to ensure that the Ragnarök would also be a safe vehicle.

Figure 1: Ragnarök Prototype (Left), and the Rose-Hulman HPVT (Right)

2 Design and Innovation

As Sir Isaac Newton once said "If I have seen further it is by standing on the shoulders of giants." This statement is true for every design group. It is necessary to perform thorough background research before significant progress can be made. Before any analysis or testing was performed, research into prior art was conducted in each area of interest, and is discussed in each section. Research and innovation is more important than ever for the team as they enter the new design category: the Unrestricted Class.

2.1 Goals

At the beginning of the year, several brainstorming and review sessions were held to reflect upon the successes and failures of the team's previous vehicles while also generating new ideas for the coming year. From these reflections, a list of vehicle goals was created for the year. The principal goals are listed in Table 1.

Table 1: 2010 Vehicle Goals

Minimize weight	Minimize surface roughness
Maximize stability	Optimize crank length
Maximize forward visibility	Maintain vehicle durability
Improve ergonomics	Refine aerodynamic modeling
Maximize rider practice time	Meet ASME practicality requirements
Manufacture the fairing shape more accurately	

2.2 Constraints

A list of constraints for this year's design was also developed. These constraints expand upon the official 2010 HPVC rules. Additional constraints were based upon rules imposed by Human Powered Race America, the Rose-Hulman team's own consideration for safety, and the necessities of transporting the vehicle. Table 2 outlines these constraints.

Table 2: 2010 Vehicle Constraints

15 ft (4.57 m) minimum turning radius	Rear-view mirrors
Braking from 15 to 0 mph (24.24 to 0 kph) in < 20 ft (6.10 m)	Rider protection from sliding/abrasion
Independent and redundant braking system	No exposed carbon fiber near rider
No more than 8 ft (2.44 m) long for shipping purposes	Four point safety harness
Roll bar supporting 600 lb_f (2.67 kN) top load with elastic deflection less than 1 in (2.54 cm)	
Roll bar supporting 300 lb_f (1.33 kN) side load with elastic deflection less than ¾ in (1.91 cm)	

2.3 House of Quality

To design a vehicle for the new unrestricted class, the team used quality function deployment to evaluate the importance of new design challenges alongside those previously encountered. A House of Quality (HoQ) was chosen to organize and analyze the large number of needs and metrics pertaining to the design of the vehicle. The correlation values between each need and metric, relative importance values, and extent of influence were chosen through debate. A relative importance of greater than four indicated that the following are critical metrics: roll bar specifications met, total weight, rider fits vehicle, forward distance for sight of ground, stability, practicality features, ASME practicality score, rolling resistance, outer dimensions, fairing material, and frame material. These columns are highlighted in the HoQ. There were five pairs of significant factors with strong positive interactions that would provide the greatest benefit to the performance of the bike for the effort put into them: total weight and fairing material, total weight and frame material, practicality features and ASME practicality score, rider fits vehicle and forward distance for sight of ground, and forward distance for sight of ground and stability. To show the importance of these positive interactions the correlation paths were highlighted in the roof of the HoQ. To benchmark the desired vehicle against other competitors, a column was created to establish how well each met the customer's needs on a scale of 1 to 5. The scores given in the current competition category are based upon previous years' vehicle performances. The ratio of the planned vehicle score to the current competition score is called the improvement ratio. An improvement ratio of greater than one indicates an area where the team concentrated its efforts to improve beyond the current competition. Any need defined to have a customer importance of five received an improvement ratio of at least unity and is highlighted in the HoQ. An improvement ratio of less than unity indicates the categories in which the team consciously chose to make improvement a secondary priority, in an effort to achieve greater success overall. The HoQ is shown in Table 3.

Table 3: House of Quality

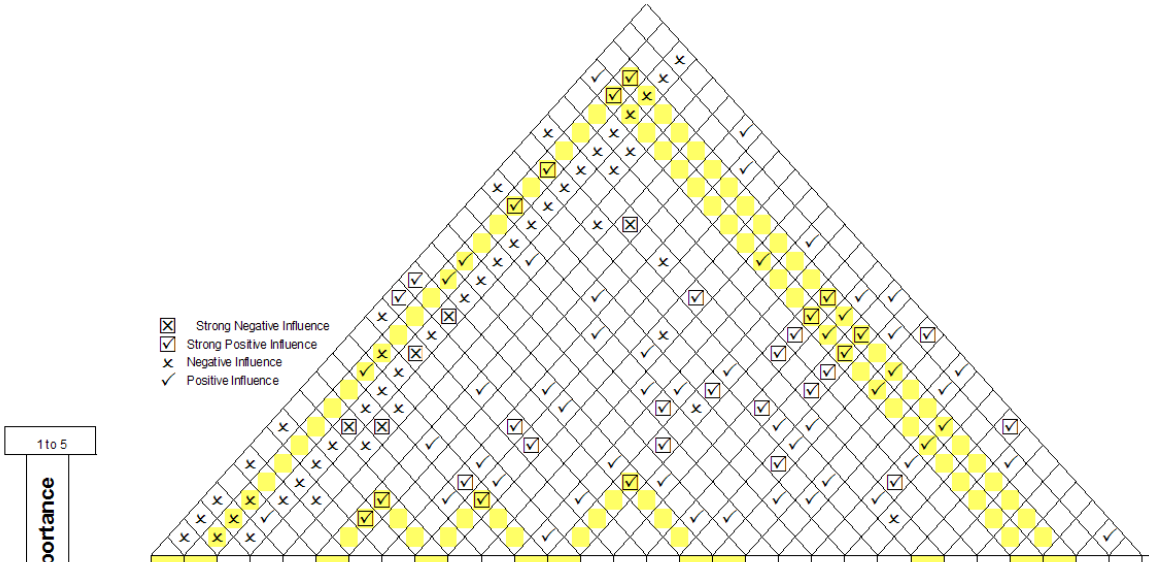

Needs	Customer Importance (1 to 5)	Metrics: Roll Bar Specifications Met	Total Weight	Time to Design	Time to Fabricate	Unused Components	Rider Fits Vehicle	Driveline Efficiency	Horizontal Field of View	Forward Distance for Sight of Ground	Drag Coefficient	Asthetically Pleasing	Stability	Practicality Features	ASME Analysis Score	ASME Safety Score	ASME Testing Score	ASME Practicality Score	Rolling Resistance	Months of the Year Usable	Down Time During Events	Acceleration	Storage Volume	Stopping Distance from 15mph	Outer Dimensions	Crank Length	Chainring Shape	Fairing Material	Frame Material	Turn Radius	Durability (Crashes Before Failure)	Current Competition	Planned Vehicle	Improvement Ratio
High Score	5	9		1	1				1	1	3	3	1	9	9	9	9	9	3	3			1	1						1	3	4	5	1.25
Light	4		9			3								1				1	3	1		3		1	1			9	9			5	4	0.80
Design is Managable	3			9	9	1		1			1	3	3	3	1	1	1	1		1	3		1			1	3	3	1	3	5	5	1.00
Construction is Managable	3	3	1	1	9	1		1			1	3	3	3	1	1	1	1	1			3	3		9		9	9	9		3	5	5	1.00
Utilizes all Components	2		3		3	9		1				1									3											5	5	1.00
Manuverable	4		3				3		3	9			9						1	3	1			1	1					9		3	5	1.67
Minimal Rider Interferance	3	1		1		1	9		3	3			3	1				1		1	1				3	1						4	5	1.25
Maximum Power Transfer	4			1			9	9	3	3	9		3						9			9				3	3	3	3			3	4	1.33
Good Field of View	4	1		1			9		9	9			3			1									1							4	4	1.00
Aerodynamic	5			1	1						9	3			3		3					9	3		9							4	4	1.00
Asthetically Pleasing	2			1	3							9		1				1			1				3			3	3			5	4	0.80
Practical	4	9	3	1	1		3		9	9	3		9	9				9	3	3	3		9	3	1			3	3	3	3	4	4	1.00
Stable	4		1	1			3		3	3			9			3					3								9		4	5	1.25
Safe	5	9	3	9	9		3		9	9			9	3		9		9		3	3			9	3			9	9	3	9	4	5	1.25
Meets ASME Safety Specifications	5	9	3	1	1		3						1	9	9	9	9	9						3				3		3		5	5	1.00
Low Rolling Resistance	4	1	3														3		9			3										4	3	0.75
Tolerates all Weather Conditions	3		1						3	3								3	1	9	1											4	2	0.50
Maintainable	3				1									3				3	1													3	5	1.67
Accelerates Quickly	4	1	3			1	1	3			9		1						9			9				3	3	3	3			4	4	1.00
Fast	4		3	3	3			3	1		9		1		1	1	3		9			3				3	3	1	1			4	5	1.25
Storage Space	3			3		1	3													3			9		9							4	4	1.00
Capable of Stopping	5		3													9		3						9						3	4	5	1.25
Free Standing	3												3	9				9														5	5	1.00
Lockable	1		1											3				3	1													5	5	1.00
Trasportable	4	1	3			1	1																1		9			1	1			4	4	1.00
Tolerates Road Obstrucitons	2		1						3	3			3					3		3										9	5	5	1.00
Durable	2	9	3	1	1											3		3	1	3		1		1				9	3		9	3	5	1.67
Low Cost	2	1	3			1						1																9	9		1	4	2	0.50
Innovative	4		1	3				1			3				3		9	3		1			1			3						4	5	1.25
Rideable in Reverse	4		1	1	1													3														5	4	0.80
Easy Ingress and Egress	4			1		1	9						9	9	1			3			9				3	1						3	5	1.67
Ergonomic	4			1			9											3									3					4	5	1.25
Absolute Importance	X	54	52	41	43	20	65	19	47	52	47	23	67	63	28	46	38	77	51	34	28	40	28	28	52	11	25	65	56	29	46	1275		
Relative Importance	X	4.2	4.1	3.2	3.4	1.6	5.1	1.5	3.7	4.1	3.7	1.8	5.3	4.9	2.2	3.6	3	6	4	2.7	2.2	3.1	2.2	2.2	4.1	0.9	2	5.1	4.4	2.3	3.6	100		
Current Competition	X	Y	45	N/A	?	0	Y	N/A	170	15	0.045	10	N/A	0	20	18	24	27	N/A	N/A	10	N/A	N/A	13	N/A	N/A	N/A	C	C	15	75			
Improvement Direction	X	▲	▼	▼	▼	▼	▲	▲	▲	▲	▼	▲	▲	▲	▲	▲	▲	▲	▼	▲	▼	▲	▲	▼	▼	►	►	▲	▲	▼	▲			
Target Value	X	Y	50	8	12	0	Y	99	340	20	0	10	N/A	N/A	30	20	35	45	2	12	0	N/A	N/A	10	N/A	N/A	N/A	C	C	10	300			
Units	X	Y/N	lbf	wks	wks		Y/N	%	deg	ft		pts							lbf	mths	min			ft					ft	crsh			

2.4 Innovation

2.4.1 Interchangeable Tilting Trike

To meet the needs of the new unrestricted class, the HPVT decided to explore the option of a tilting trike. A constant three points of contact with the ground and the ability to lean into turns give this design the skid recoverability and low-speed stability of trikes with the high speed handling of single track vehicles. The works of HPV designers Dennis Grelk, Tim Hicks, and Rick Wianecki were studied to get an idea of how experienced competitors in the Human Powered Race America (HPRA) competitions have developed tilting recumbent trikes.

The HoQ indicated that the largest areas for improvement over previous vehicles and the most important new concerns were in stability and vehicle practicality. In order to keep the rolling resistance and aerodynamics of a two wheeled vehicle, but gain the stability and traction advantages of a tilting trike, a convertible tilting trike design was selected, allowing the vehicle to switch from two to three wheels. To the team's knowledge, the Ragnarök is the first streamliner, interchangeable tilting-trike ever to be developed. This decision presented some unique challenges. The problem was approached using modular design, with the two wheeled platform and the bolt on assembly designed separately. Brainstorming resulted in a design with a four bar linkage, using three vertical tubes to attach the wheels and drop outs to a horizontal steel flat bar and tie rods. The prototype is shown in Figure 2.

Figure 2: Prototype of interchangeable tilting trike assembly

The initial design used bushings to link the horizontal structural members to the vertical square tubes. Over time, these became worn and loose. In order to solve this problem on the final design, the bushings were replaced with bearings pressed into the horizontal members. The final design also incorporates brakes, which were not needed for testing on the prototype. The braking force was calculated to be a large source of stress on the tilting trike assembly, as described in Section 3.1, leading to further iterations of the design. Three iterations were developed until the design was finalized. The three iterations are shown in Figure 3.

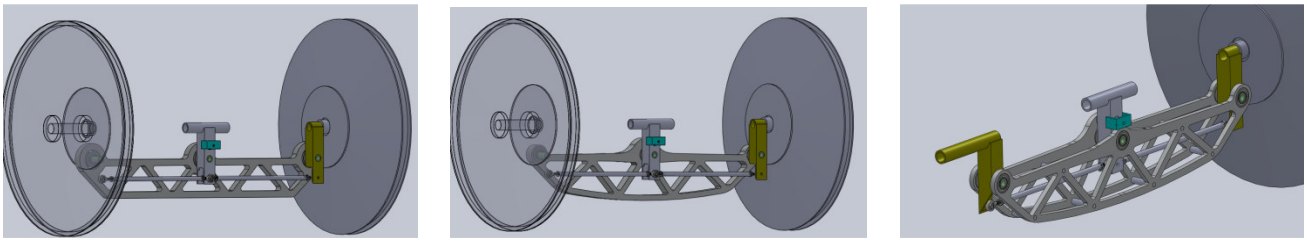

Figure 3: (left to right) Iteration 1 - Square Truss, Iteration 2 - Rounded Truss, Iteration 3 - Double Rounded Truss

The initial goal of the design was to arrive at a FoS of 3 using a design that could be easily manufactured with a water jet cutter to preserve the heat treatment of the material. The first iteration utilized a single square truss of 6061-T6 aluminum to support 3 pairs of bearings pressed in from each side at each vertical post; six bearings in total. This design had a factor of safety (FoS) of 5.4 when turning, but when the braking torques and forces were applied the FoS dropped to 2.1. The second truss iteration had a curved bottom member with a taper in all the members as they approach the vertical columns attached to the wheels. This design had slight improvement, but still had a low FoS of 2.4. The final iteration used two separate aluminum trusses with the bearings pressed in from only one side. Two plates of 3/8 in (0.95

cm) 6160-T6 aluminum were water jet cut to form the two truss pieces and 3/16 in (0.48 cm) wall 6160-T6 aluminum tube was used to form the vertical columns. When tested with Finite Element Analysis (FEA) the third iteration showed marked improvement and FoS of 3.1.

2.4.2 Locking Mechanism

A locking mechanism was developed in order to meet the goal of developing a free standing vehicle and to help the rider enter and exit the vehicle quickly and safely. This mechanism was designed into the tilting trike assembly by adding a locking pin, as demonstrated in Figure 4, that the rider can control with a shift lever.

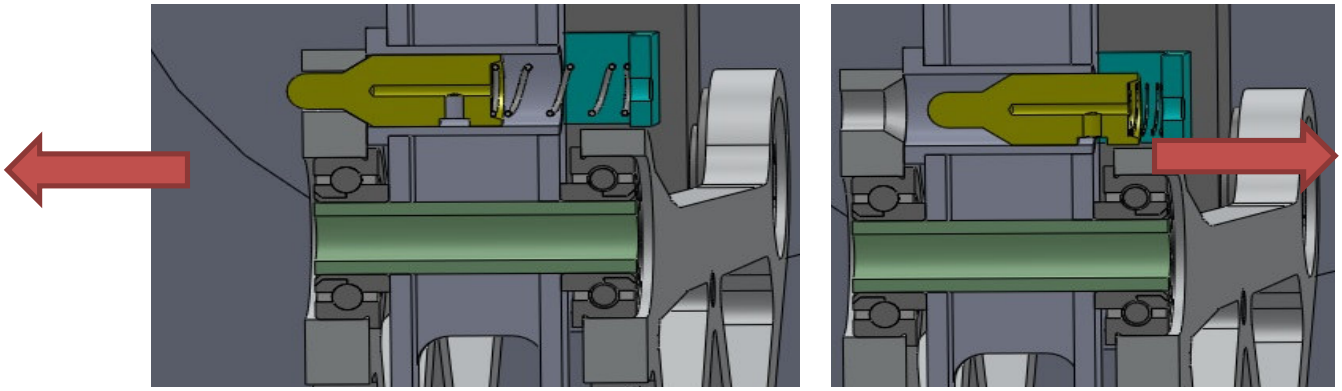

Figure 4: Cross Section of Trike Upright Locking Mechanism with pin engaged (locked upright, left) and pin removed (free to tilt, right)

The pin is removed by shifting the lever once the vehicle is in motion. When the rider desires to stop the lever is released and the spring loaded pin contacts the rear truss. When the rider leans back to vertical the pin is pushed into the hole in the rear truss and locks it in place when fully engaged. This allows the rider to come to a complete stop and start without assistance and to exit the vehicle at their convenience without the vehicle tipping over.

2.4.3 Fairing Shape Development

The fairing was designed to be as aerodynamic as possible without interfering with the motion or vision of the rider. To ensure appropriate clearances, a CAD model of the volume occupied by the rider and internal components, seen in Figure 5, was developed from data collected using 3-dimensional motion capture equipment. This process is described in Section 4.3. Instead of developing models and then verifying that the rider would fit, this new method allowed fairing models to be drawn relative to the space required by the rider, ensuring an improved fit.

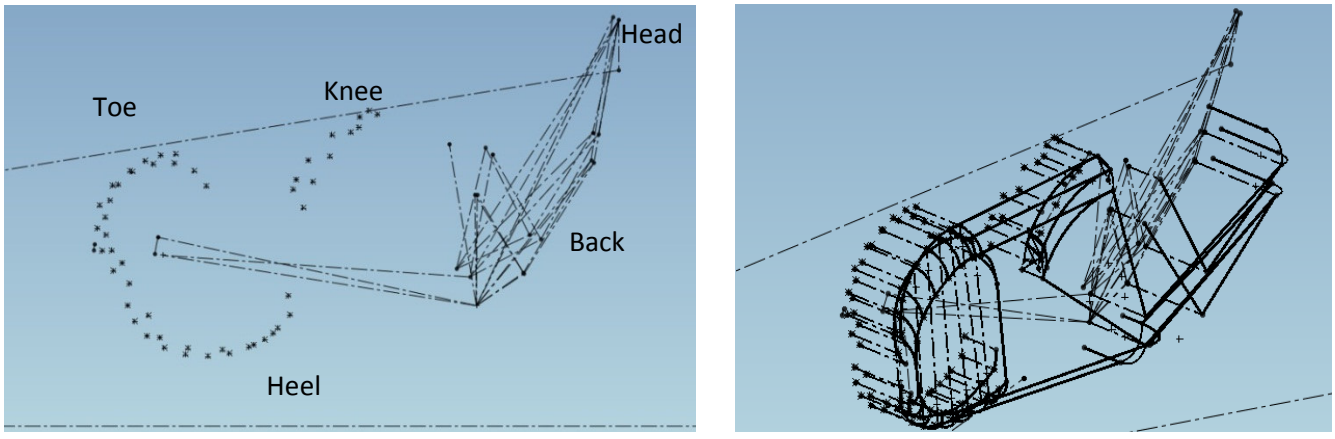

Figure 5: Rider Space Model

The rider's seat angle was rotated upright by 5° relative to the 2009 Mark IV, improving the field of view as described in Section 5.2. Testing conducted during the development of the 2009 Mark IV indicates that this more vertical position also allows riders to output slightly more power. A more refined shape allows for a $C_d A$ comparable to that of the 2009 Mark IV despite the increased frontal area necessary to improve rider visibility and fairing clearances, as described in Section 3.6.

Additional constraints on the fairing were determined from past experience and engineering considerations, after which a Computational Fluid Dynamics (CFD) program was used to analyze and iteratively refine the fairing model. Using the maximum lean angle of 45° from the 2009 Mark IV, observation of riders on the prototype, and allowing for a 2° tolerance, a maximum lean angle of 47° was chosen to prevent the fairing from hitting the ground. A separate model of the tilting trike assembly was used to validate that the wheels would not strike the fairing when turning. A large integrated windshield was ruled out due to issues with poor optical characteristics and elevated internal temperatures as in the 2007 R5. To accommodate riders of different heights, an interchangeable seat system was chosen, as described in Section 2.4.5. The overall length of the vehicle was kept less than 8 ft (2.44 m) to reduce shipping costs.

2.4.4 Rib and Skin development

In order to design a lighter vehicle, the team explored several different options for the fairing. The main ideas considered were: separate frame with a nonstructural fairing (similar to the 2007 R5), continuous core (similar to the 2008 Infinity), and ribbed tub frame (similar to the 2009 Mark IV). It was decided that the best way to reduce weight and cost while maintaining performance and safety was to improve upon the design of the Mark IV, which utilized a ribbed tub frame design. The Mark IV was unnecessarily heavy because it was the HPVT's first attempt to construct a ribbed tub frame vehicle. This year, the team has significantly reduced the weight of the vehicle overall while still maintaining the aerodynamic and structural properties of its stronger but heavier predecessor.

The Ragnarök will have a thinner skin between the ribs which is not intended to be structural. The rib structure for the Ragnarök is shown in Figure 6.

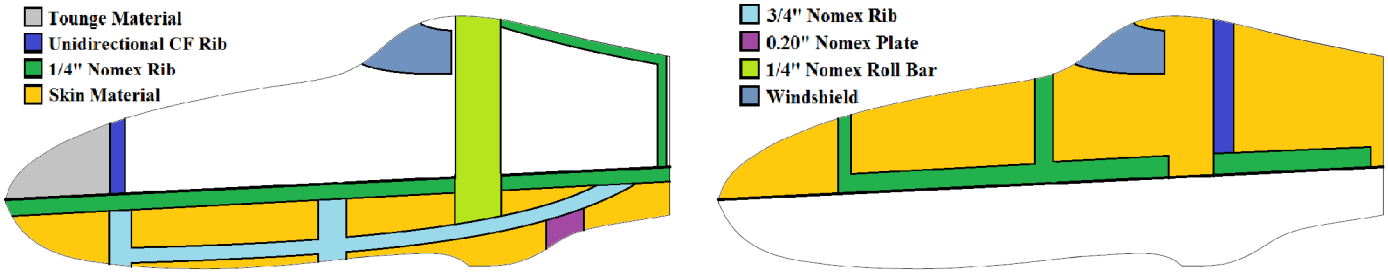

Figure 6: Bottom and Top Rib Structure

Visual analysis of the Mark IV also revealed that the areas where the fairing was significantly marred by contact with the ground during falls were highly localized. Wear resistant fabric is not needed in areas that do not contact the ground. Therefore only the portions of the fairing that will contact the ground in the event of a crash will be covered in wear resistant carbon/Kevlar hybrid fabric. Figure 7 indicates the significant wear zone from the Mark IV.

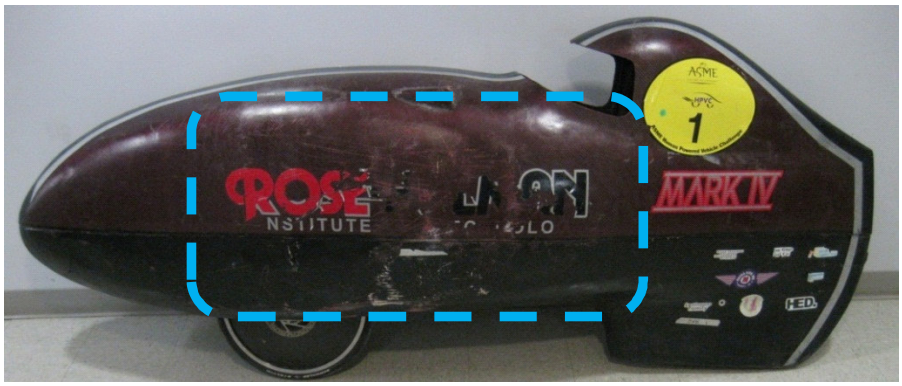

Figure 7: 2009 Vehicle Mark IV Skid Zones

In addition, a new material called Zylon, a type of aramid fabric, was tested to determine if it had better wear resistance than the hybrid fabric. The specific testing methods and results are discussed in Section 4.6. Zylon was not found to have significantly better wear resistance so it was decided to continue the use of hybrid fabric in the high wear zones on the skin of the vehicle. In order to determine the skin material, twelve possible samples were laid up in the same manner used for construction of the vehicle. These samples were subjected to a permeability test in order to determine if water would be able to pass through them. If the samples were watertight then they would be less likely to have holes which would allow air to pass through the fairing. After three minutes, if water had passed through the sample then the

sample failed that test and would not be considered as a possible skin. These samples and the results are shown in Table 4.

Table 4: Skin Samples

Carbon Layer	Inner Layer	Permeability	Combined Weight
5.5 osy (186 gsm)	NA	Fail	5.5 osy (186 gsm)
8.3 osy (281 gsm)	NA	Fail	8.3 osy (281 gsm)
11 osy (373 gsm)	NA	Fail	11 osy (373 gsm)
5.5 osy (186 gsm)	4 osy (136 gsm) Kevlar	Fail	9.5 osy (322 gsm)
8.3 osy (281 gsm)	4 osy (136 gsm) Kevlar	Pass	12.3 osy (417 gsm)
11 osy (373 gsm)	4 osy (136 gsm) Kevlar	Fail	15 osy (509 gsm)
5.5 osy (186 gsm)	4 osy (136 gsm) Zylon	Fail	9.5 osy (322 gsm)
8.3 osy (281 gsm)	4 osy (136 gsm) Zylon	Pass	12.3 osy (417 gsm)
11 osy (373 gsm)	4 osy (136 gsm) Zylon	Fail	15 osy (509 gsm)
5.5 osy (186 gsm)	6 osy (203 gsm) Zylon	Pass	11.5 osy (390 gsm)
8.3 osy (281 gsm)	6 osy (203 gsm) Zylon	Pass	14.3 osy (485 gsm)
11 osy (373 gsm)	6 osy (203 gsm) Zylon	Pass	17 osy (577 gsm)

All of the 6 osy (203 gsm) inner layer skin samples passed the test as well as all of the 8.3 osy (281 gsm) carbon samples. The 4 osy (136 gsm) Kevlar and Zylon samples were eliminated after the results of the carbon shard testing detailed in Section 4.7. Of the remaining samples, the 5.5 osy (186 gsm) carbon sample was considered too easily deformable and therefore eliminated. The 11 osy (373 gsm) carbon sample was significantly stiffer than the 8.3 osy (281 gsm) carbon sample and also slightly cheaper because it was 2x2 twill instead of the 4x4 twill of the 8.3 osy (281 gsm) carbon. Thus, for each quarter section, there is a continuous skin layer composed of 11 osy (373 gsm) carbon fiber on the outside followed by 6 osy (203 gsm) Zylon near the rider. On the outside of the carbon in the high wear areas there would be a single layer of hybrid fabric. This resulted in a significant reduction in weight compared to the previous year's vehicle. The ribbed tub frame and top fairing had a combined weight about 34 lb_f (151 N) as opposed to the approximately 50 lb_f (222 N) of the Mark IV.

2.4.5 Improved Seat

To meet the design goal of accommodating riders of different heights, the Ragnarök features two custom molded seats. The vehicle contains a large seat for tall riders and a smaller second seat that acts as a removable booster seat for shorter riders. In its installed position, the smaller seat orients the rider's hip 2.85 in (72.5 mm) higher and 0.68 in (17.2 mm) farther forward than the larger seat. This orientation allows the team's range of riders to be closer to optimum fit, maximizing rider field of view and minimizing rider interference.

The smaller seat attaches on the face of the larger seat using Velcro and is spaced apart from the primary seat at the proper orientation with foam. This attachment mechanism was chosen because it is compact and enables rapid ingress and egress. The smaller seat is lightweight and flexible by itself but is designed to obtain satisfactory stiffness by being form-fitting into the larger seat.

The seats were custom molded using sand impressions which were formed from the largest and smallest riders' backs when actively cycling. For greater breathability and heat dissipation, the larger seat has holes milled along the lumbar region. These holes assist in rider cooling during hotter rides yet their location keeps the rider clean during wetter

weather. The smaller removable seat has ribs of closed cell foam permanently bonded to the surface for rider cooling. These ribs create air channels oriented along the length of the back that assist in heat and sweat dissipation.

2.4.6 Bike Computer/Electronics

A custom cycling computer was developed to be mounted in the vehicle with a display on the exterior of the vehicle, where riders can see it without adverse effect to aerodynamics. Speed and cadence are displayed on two LED bar graphs integrated into the fairing under the mirrors. Although less precise than a standard numerical display, this display requires less of the rider's attention to get an idea of the vehicle's speed. This electronic system also incorporates head and tail lights, as described in Section 5.3. For riding with the top off, an RJ45 jack provides electrical connection for a frame mounted cycling computer.

2.4.7 Front Wheel Hole Covering

According to Sam Whittingham, the speed record holder for human powered vehicles, “The wind resistance caused by [the two wheel openings]… is equal to the rest of the bike combined” [1]. While this is most likely conjecture on his part, it does highlight the fact that the front wheel hole is a significant source of aerodynamic losses. In an attempt to minimize this, the team will be stretching Latex over the front hole, so as to create a smaller, adaptable opening that will move with the wheel. This will make the vehicle more streamlined and decrease aerodynamic losses.

3 Analysis

An important part of any design process is analysis, the examination of specific components of a complex problem to gain insight into the larger problem which can result in a closer to optimum solution. Several areas were identified for analysis: aerodynamics, structures, and vehicle performance. For the aerodynamics, a better understanding of the wind conditions was developed and then used to analyze the drag on the model in a CFD program. Also, the relative magnitude of the pressure drag and the skin friction drag was analyzed to determine the dominant force. Structural analysis included simplified hand calculations and FEA of the stresses encountered by the roll bar and the tilting trike apparatus to ensure that these features would withstand the rigors of the ASME HPVC. Finally, the drivetrain of the vehicle was analyzed to determine the optimum gear ratios for the competition.

3.1 Truss Analysis

To ensure that the tilting trike assembly would be robust enough to survive the loads it would see during operation, FEA was performed using ANSYS Workbench. A free body diagram, shown in Figure 8, was used to determine the loading conditions.

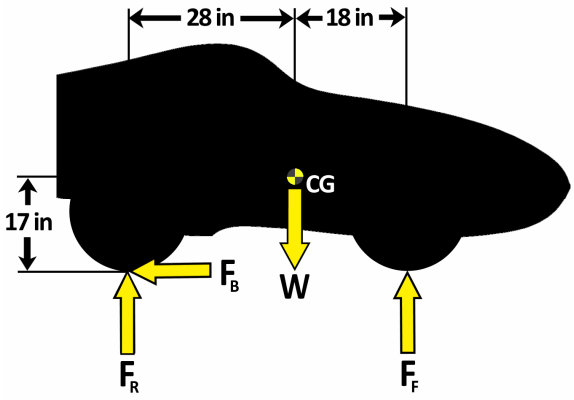

Figure 8: Free Body Diagram

The forces on the vehicle were determined for two different loading situations: maximum braking and maximum turning. The maximum combined weight of the rider and the vehicle was estimated to be 240 lb_f (1068 N).

According to calculations using the principles of conservation of linear and angular momentum, when the rear brakes are not being applied, the normal force on the rear wheel is 93.9 lb_f (418 N). However, the normal force on the rear wheel is reduced to 68.6 lb_f (305 N) when a maximum braking force of 68.6 lb_f (305 N) is applied. This assumes that the maximum braking force is equal to the normal force times a coefficient of friction of one. This also assumes that only the rear brakes are being applied. If the front brakes are also applied, the normal force on the rear wheel will be further reduced.

The FEA focused on analyzing the truss which connects the two wheels to the vehicle frame. The top of the truss is tilted 10.6° away from the rider, as detailed in Section 4.1. Since the truss and the loads applied to it are symmetric, only half of the truss was analyzed. The truss was constrained for zero displacement from the plane of symmetry. The center hole, from which the truss will be mounted to the vehicle frame, was fixed. All loads on the truss were doubled to account for the dynamic loading and applied at the hole from which the axle mounting component connects.

The FEA was performed for both the maximum braking and maximum turning situations. In the maximum braking situation, there is an upward vertical force of 68.6 lb_f (305 N) and a horizontal force of 68.6 lb_f (305 N) normal to the face of the truss. There is also a torsional moment applied to the truss, equal to the braking force times a moment arm of 7.4 in (18.8 cm), or 504.7 in-lb_f (57.0 N-m). When the bike is turning, it is possible that the bike could tip, putting all of the rear weight on a single wheel. Therefore, in the maximum turning situation, a load of 187.8 lb_f (835 N) due to the vehicle weight is applied in the upward, vertical direction. A force of 187.8 lb_f (835 N) due to the friction when turning is applied in the horizontal direction along the plane of the truss.

The FEA and the accompanying hand calculations for the turning situation resulted in factors of safety greater than five for all truss designs considered. Therefore, the rest of the analysis is focused on the more demanding braking situation.

Multiple designs for the truss were evaluated as discussed in Section 2.4.1. The FoS on the truss increased with each iteration, as shown in Table 5. The design with the largest FoS, the double truss, will be used in the final construction of the vehicle.

Table 5: Factors of Safety

	Single Truss, version 1	Single Truss, version 2	Double Truss
Factor of Safety	2.1	2.4	3.1

To ensure that the FEA was providing accurate results, a simplified model of the truss, represented as a single beam with the same outer dimensions as the truss, was analyzed. This allowed for a comparison of FEA results to hand calculations. To further investigate the behavior of the truss, each force was also evaluated individually. An example of this process for the chosen design, the double truss, is shown in Table 6.

Table 6: FEA and Hand Calculation Results

	Simplified Model Hand Calculation		Simplified Model Beam Elements		Simplified Model Brick Elements		Double Truss, Detailed Model		
	d, in (mm)	σ, psi (MPa)	d, in (mm)	σ, psi (MPa)	d, in (mm)	σ, psi (MPa)	d, in (mm)	σ_{Pin}, psi (MPa)	σ_{Truss}, psi (MPa)
Weight	0.002 (0.05)	1095 (7.55)	.002 (0.05)	1095 (7.55)	0.0023 (0.06)	1970 (13.58)	0.005 (0.13)	5053 (34.84)	2727 (18.80)
Braking Force	0.145 (3.68)	7806 (53.82)	0.142 (3.61)	7807 (53.8)	0.137 (3.48)	8570 (59.09)	0.017 (0.43)	18923 (130.47)	5773 (39.80)
Braking Moment	-	3013 (20.77)	-	-	0.036 (0.91)	3378 (23.29)	0.02 (0.51)	24955 (172.06)	10683 (73.66)
Combined Loading	-	9396 (64.78)	-	-	0.173 (4.39)	13728 (24.65)	0.016 (0.41)	24963 (172.11)	13080 (90.18)

The same symmetry assumption used for modeling the trusses was applied to the simple beam model, creating a cantilever beam system. Displacements were calculated for normal and braking forces using common Euler beam equations for cantilever beams. Bending stresses created by the normal and braking forces were also calculated. To calculate the torsional stresses experienced by a rectangular beam, Equation 1 was used, where "a" is half the length of the largest side and "b" is half the length of the smaller side [2].

$$\tau_{rectangular} = \frac{3T}{8ab^2}\left[1 + 0.6095\left(\frac{b}{a}\right) + 0.8865\left(\frac{b}{a}\right)^2 - 1.8023\left(\frac{b}{a}\right)^3 + 0.9100\left(\frac{b}{a}\right)^4\right] \quad \text{Equation 1}$$

The double truss configurations puts columns of 2024-T4 aluminum between the trusses which serve to take up much of the braking force stress and make the trusses less prone to deformation caused by the braking moment. The trusses perform very well in tandem, only coming under a stress of 13 ksi (89.6 MPa) which results in a FoS slightly greater than three. The maximum stress of 13,080 psi (90.2 MPa) is shown as the red spot in Figure 9 on the right.

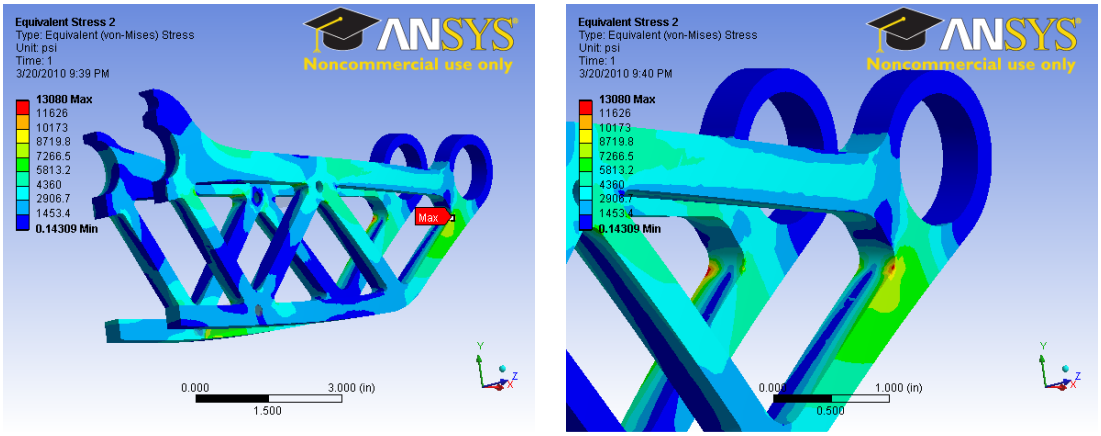

Figure 9: Truss Von-Mises Stress

The pins were a modeling concern in FEA because of very small stress concentrations where the face of the pin met the truss. Nearly the entire pin sees a stress less than 16 ksi (110 Mpa), but the stress concentrations are unable to converge in the ANSYS model. This is an artifact of applying loads to an increasingly small surface. If the pin were to plastically deform in these localized concentrations there would not be a loss of the properties in the double truss assembly. The small scale of the high stresses can be seen in Figure 10.

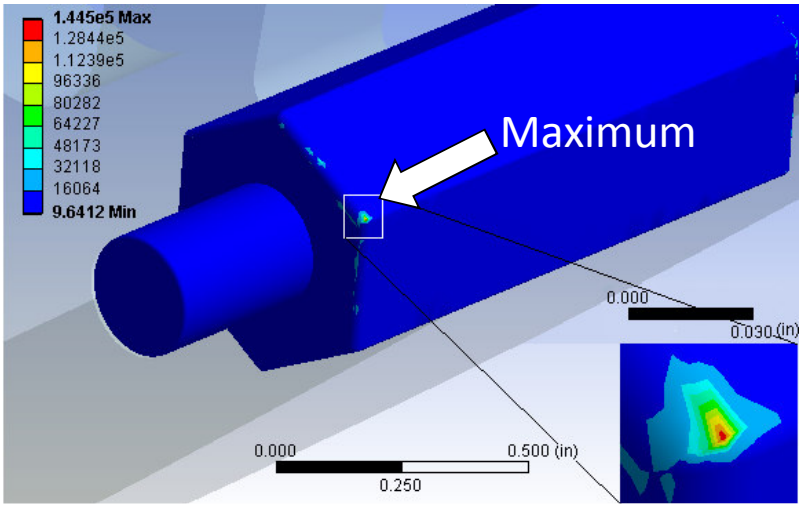

Figure 10: Pin Von-Mises Stress in psi

3.2 Drivetrain Analysis

Riders pedal most efficiently while at a certain cadence (pedal revolutions per minute). Each rider has a preferred cadence, which could vary based on the amount of power the rider is trying to supply. Also, any given race will require gears for low speeds when accelerating from rest or after turns, and will require high speed gears during sprints. It is advantageous to accommodate all possible speeds and cadences, but the Ragnarök is limited to 9 gears.

The Ragnarök features a two-chain drivetrain. One chain connects the pedals to a mid-drive, and another chain connects the mid-drive to the cassette on the wheel. The gearing ratio of this mid-drive can be changed to optimize the gears available for each event. The best method for determining the mid-drive gearing ratio is to define a maximum desired speed for each event and a minimum cadence at which riders are expected to reach this speed. A mid-drive ratio should be chosen such that the highest gear on the cassette accommodates this speed and cadence. This method gives an ideal range of gears by finding the slowest gear ratio such that no rider will need to shift above the fastest gear on the cassette.

A maximum expected speed of 45 mph (20.1 m/s) was chosen for the drag race event, and the minimum cadence at which a rider is expected to reach this speed is 110 rpm. These numbers dictate a best mid-drive ratio of 1.36. The maximum expected speed for the speed endurance race event is 35 mph (15.6 m/s) at a minimum cadence of 100 rpm. This dictates a mid-drive gearing ratio of 1.17 for the endurance event. For the utility endurance event, a maximum speed of 30 mph (13.4 m/s) and a minimum cadence of 95 rpm are expected, dictating a gearing ratio of 1.05. The actual mid-drive gear ratios will be fine-tuned through testing before each event.

3.3 Cost

The material cost of the Ragnarök was approximately $2,066 for a total of $247,910 per year assuming a production volume of 10 vehicles per month. Including salaries the net expenses for each year is approximately, $499,000. The first year an initial investment of $15,579 will be required for capitol such as machines and tools. If the per vehicle sale price is set at $4,895 and the sales volume exactly matches the production volume, this would result in an average yearly profit of $85,333 over the first six years. The total profit over the first six years in Net Present Value would be approximately $464,302. The details of this analysis are shown in Appendix 1.

3.4 Wind Condition Analysis

The apparent wind angle experienced by a moving vehicle is a combination of the wind direction and the vehicle's motion. A cross-wind will become less significant as a vehicle travels at faster speeds. To ensure that the fairing was designed to be effective at the apparent wind angle likely to be encountered in competition, a MATLAB program was written to determine the weighted probability of each apparent wind angle. This program used a distribution of wind speeds and vehicle speeds, in order to determine the probability of each apparent wind angle. The square of the airspeeds was used as the weighting factor for this calculation because the drag force is proportional to the square of velocity. The vehicle speed distribution, based on the competition performance of the team's past two vehicles, is as seen in Equation 2, with terms estimating male and female endurance and sprint speed distributions, where $f(V_{vehicle}, \mu, \sigma^2)$ is the normal distribution with mean μ and variance σ^2, and the H is the Heaviside function. The wind speed distribution was taken to be the sum of the Rayleigh distributions whose means occurred at the mean wind speed for each of the competition locations [3]. This is shown in Equation 3. The Rayleigh distribution is used in wind engineering when only mean wind speeds are available [4,5,6]. The resulting cumulative distribution of the apparent wind angle is shown in Figure 11, demonstrating that 90% of the expected winds occur at an angle less than 23.4°. Based on this analysis, each fairing design was tested without crosswind and with a crosswind that produced a 23.4° apparent wind angle, as described in Section 3.6.

$$Speed\ Probability = f(V_{vehicle}, 17.85, 2.25^2) + f(V_{vehicle}, 15.5, 2.25^2) + H(46 - V_{vehicle}) + H(36 - V_{vehicle}) \quad \text{Equation 2}$$

$$Wind\ Probability = 0.177 \cdot V_{wind} \cdot e^{-0.016 \cdot V_{wind}^2} + 0.144 \cdot V_{wind} \cdot e^{-0.010 \cdot V_{wind}^2} \quad \text{Equation 3}$$

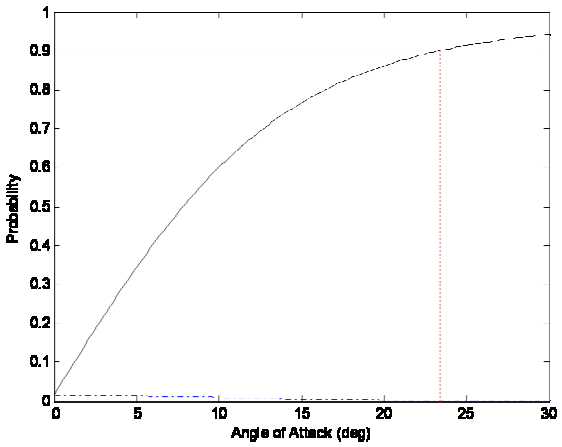

Figure 11: Wind Angle Significance

3.5 Skin Friction Analysis

The fully faired human powered vehicle is designed to reduce the aerodynamic losses associated with the pressure drag existent on a traditional recumbent racing vehicle. Pressure drag results from the difference in pressures between the front and rear of the vehicle. Air at the front of the vehicle will have a high pressure as a result of stagnation. If the air flow stays attached to the vehicle, the pressure at the rear of the vehicle will be similar to the pressure at the front. When flow detaches from the vehicle a volume of low pressure air is created between the flow and the vehicle. This difference in pressure results in a rearward force on the vehicle. Unfortunately, while a fairing reduces pressure drag it also adds skin surface area that induces its own surface drag. This drag is a result of the shear force caused by the relative velocity difference between the fairing and the air. In order to design a fairing with minimal overall aerodynamic losses simple hand-calculations were used to determine what factor, skin friction or pressure drag, dominates the drag on HPV fairings.

The overall drag force can be calculated using the 2009 Mark IV's maximum speed and associated power output. Equation 4 relates the power output to the velocity of the vehicle.

$$P = C_d A_{frontal} \rho \frac{V^3}{2} \qquad \text{Equation 4}$$

The overall effect of drag force on the vehicle was calculated from Equation 5 and was calculated at the Mark IV's 45 mph sprint racing speed.

$$F_d = C_d A_{frontal} \rho \frac{V^2}{2} \qquad \text{Equation 5}$$

Hence, the overall drag force on the Mark IV is 3.75 lb_f (16.6 N). This force has three primary components, aerodynamic losses, rolling resistance, and drivetrain losses. The rolling resistance was calculated to be 1.11 lb_f (4.9 N) based on manufacturer's specifications for the tires. If the drivetrain losses are considered negligible then the overall drag force is expressed by Equation 6.

$$F_d = F_{d,\ rr} + F_{d,\ aero} \qquad \text{Equation 6}$$

The drag force induced by aerodynamic losses is composed of skin friction and pressure drag from the body and additional aerodynamic losses from the wheels, as demonstrated in Equation 7.

$$F_{aero} = F_{d,\ skin} + F_{d,\ pressure} \qquad \text{Equation 7}$$

Drag induced by skin friction forces can be modeled by assuming that the vehicles skin approximates a flat plate. Skin friction depends on the shear stress induced by the type of flow in the boundary layer. Two extremes can be used for this comparison, either assuming that the flow is entirely laminar or fully rough turbulent along the length of the vehicle. The equation that assumes completely laminar flow is reproduced in Equation 8.

$$C_{f,laminar} = \frac{1.33}{\mathrm{Re}_L^{\frac{1}{2}}} \qquad \mathrm{Re}_L < 5 \times 10^5 \qquad \text{Equation 8}$$

This estimation of the skin friction can be used in Equation 9 to calculate the drag force caused by the skin.

$$F_{d,\ skin} = C_{f,\ skin} A_{skin} \rho \frac{v^2}{2}$$ Equation 9

The fully laminar approximation estimates the smallest skin friction value of 5.93% of the total aerodynamic drag. The largest skin friction value can be estimated by assuming that the vehicle is fully rough turbulent flow along the entire vehicle and is demonstrated by Equation 10.

$$C_f = \left(1.89 - 1.621 \log \frac{\varepsilon}{L}\right)^{-2.5}$$ Equation 10

The largest skin friction value estimate, assuming fully turbulent flow, is 18.2% of the total aerodynamic drag.

The overall skin friction calculation can be improved by determining the transition location between laminar and turbulent flow. Hence, the overall skin friction is calculated by integrating the local skin friction coefficient, $C_{f,\ L}$, over the surface of the vehicle as demonstrated by Equation 11.

$$C_{f,\ skin} = \frac{1}{L}\left(\int_0^{L_{cr}} C_{f,L,laminar}\, dL + \int_{L_{cr}}^{L} C_{f,L,turbulent}\, dL\right)$$ Equation 11

The critical length that determines the transition region between laminar and turbulent flow is dependent upon the situation. A common assumption is that the flow is laminar from the front of the vehicle to the point where the Reynolds number exceeds $5x10^5$. Equation 12 is a simplification of Equation 11 with the transition location at Re = $5x10^5$.

$$C_{f,\ skin} = \frac{0.074}{\mathrm{Re}_L^{\frac{1}{5}}} - \frac{1742}{\mathrm{Re}_L}$$ Equation 12

For the Mark IV, this indicates that the transition region is 14.5 in (0.268 m) from the nose of the vehicle. According to tuft testing, see Section 4.5, the transition between laminar and visually turbulent flow occurs at the head bubble which is 5.25 ft (1.6 m) from the nose. Therefore, this transition location was used instead of the commonly accepted location found using a Reynolds number of 5 x 10^5. The four drag coefficients, associated drag forces and percentage of overall drag induced by skin friction are summarized in Table 7.

Table 7: Summary of Skin Friction Drag Approximations

	$C_{f,\ skin}$	$F_{d,\ skin}$ lb_f (N)	% of $F_{d,aero}$ due to Skin Friction
Fully Laminar	0.00073	0.155 (0.70)	5.9%
Fully Turbulent	0.0038	0.815 (3.63)	31.1%
Transition at Re= 5 x 10^5	0.0031	0.668 (2.97)	25.5%
Transition at Head Bubble	0.0016	0.348 (1.55)	13.3%

According to the skin friction calculations with a transition location at the head bubble, the skin friction is approximately 13% of the overall aerodynamic drag. This conclusion supports the basis for the fairing design emphasis on minimizing pressure drag more than minimizing surface area.

3.6 Aerodynamic Analysis

After physical modeling in SolidWorks was completed, the aerodynamic characteristics of each model were analyzed using COSMOS FloWorks for CFD analysis in order to minimize the aerodynamic losses. This year, due to the change from the sprint competition to the lower speed drag race format, it was decided that the vehicles performance in a cross wind scenario would be an important factor. Due to the relatively low speeds at the ASME HPVC events, expected to be between 0 and 35 mph this year, a mild breeze can create a significant change in the aerodynamic properties of the vehicle by altering the apparent wind angle. These factors led to a testing program in which all models were tested in both a zero crosswind scenario and a 23.4° apparent wind angle scenario. Testing in this manner means that the results will be asymmetric, so a plane of symmetry was not used during the analysis. Flow trajectories from the crosswind scenarios are shown in Figure 12. A large turbulent bubble is present on the lower tail section of the Mark IV and the turbulence off the head bubble is more significant.

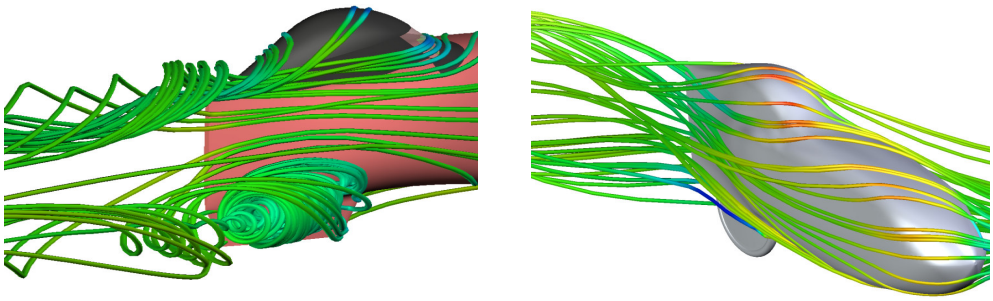

Figure 12 Crosswind Flow Trajectories for the Mark IV (Left) and the Ragnarök (Right)

The initial model was created using the points gathered from the motion capture data collected earlier and from the past experience of the aero design team. Using tools in FloWorks such as surface plots and flow trajectories, the models were examined and areas for improvement were selected and adjusted. This process was repeated several times until a suitable solution was reached. This year, models were tested using a higher rear wheel fairing and rear disc wheel in order to cut down on cross sectional area and reduce drag. The vehicle's nose was also lowered as much as the results of the motion capture data would allow, and the tail was raised to keep flow from detaching behind the head bubble. In addition, this year's nose is more rounded to provide more space for the rider's feet while the sides are nearly flat in order to keep cross sectional area to an absolute minimum. Using the drag force values calculated in each of the FloWorks simulations, the C_dA was calculated using Equation 5. Table 8 shows the results of the CFD analysis. Since the vehicle is more likely to be encountering a head on wind scenario it was given a weight of 2/3, rather than 1/2, for the combined C_dA. The resulting combined C_dA for the Ragnarök is lower than prior iterations despite a larger frontal area.

Table 8: Summary of CFD Results

Model	Area, $ft^2(m^2)$	Drag Force, $lb\ (N)$		$C_dA,\ ft^2\ (m^2)$		
		Headwind	Crosswind	Headwind	Crosswind	Combined
2009 Mark IV	3.57(0.33)	1.43(6.36)	1.84(8.18)	0.268(0.0249)	0.345(0.0321)	0.294(0.0273)
Initial Model	3.94(0.37)	2.55 (11.3)	2.43(10.8)	0.478(0.0444)	0.457(0.0421)	0.471(0.0436)
2010 Ragnarök	4.06(0.38)	1.46(6.49)	1.59(7.06)	0.274(0.0254)	0.298(0.0277)	0.282(0.0262)

3.7 Roll Bar Analysis

Two separate types of analysis were used in an effort to ensure accuracy in roll-bar deflection estimates for both of the roll bar tests, the side load as well as the top load. The first was by simple hand calculations based on beam bending equations, and the second was through the use of finite elements employing ANSYS Workbench. The values are all compared in Table 9 at the end of this section.

3.7.1 Hand Calculations

The simple roll bar loading conditions for the hand calculations are shown in Figure 13. The red arrows are the applied loads and the bottom of each model is constrained to the ground.

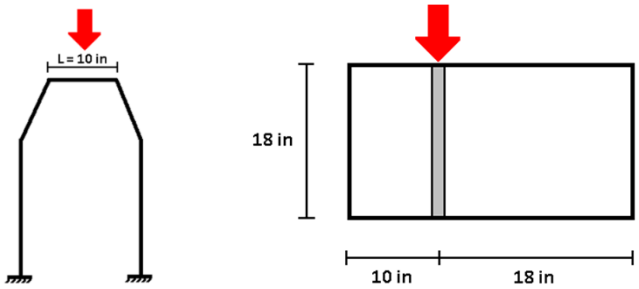

Figure 13: Roll Bar Top Load (Left), Side Load (Right)

The required load of 600 lb_f (2.67 kN) was applied at the center of the ten-inch bar. Any deflection from the side walls is likely to be negligible for this analysis. The second moment for the bar was found and the deflection was calculated using a standard beam bending equation for a simply supported beam, Equation 13.

$$y_{max} = -\frac{PL^3}{48EI}$$ Equation 13

The side load test was modeled as shown in Figure 13, a frontal view of the roll bar on its side. The top bar as well as the center bar (actually a tube) both had deflections calculated independently using the required 300 lb_f (1.33 kN) load, and the minimum deflection of these two was assumed to be a safe estimate of the total deflection. The beam deflection calculation used an equation similar to Equation 13, and the deflection of the center tube was found using Equation 14, a spring-deflection equation.

$$y_{deflect} = \frac{PL}{EA}$$ Equation 14

3.7.2 Finite Elements

A more accurate model of the roll bar was constructed and imported into ANSYS Workbench and the required loads were applied at the specified angles and positions. The side of the model opposite the loading was fixed. The deflections are reported in Table 9. Figure 14 shows results of the analysis.

Table 9: FEA and Hand Calculation Results

	Hand Calc. Results, in (mm)	ANSYS Workbench, in (mm)
Top Load	0.138 (3.51)	0.119 (3.02)
Side Load	0.005 (0.13)	0.009 (0.23)

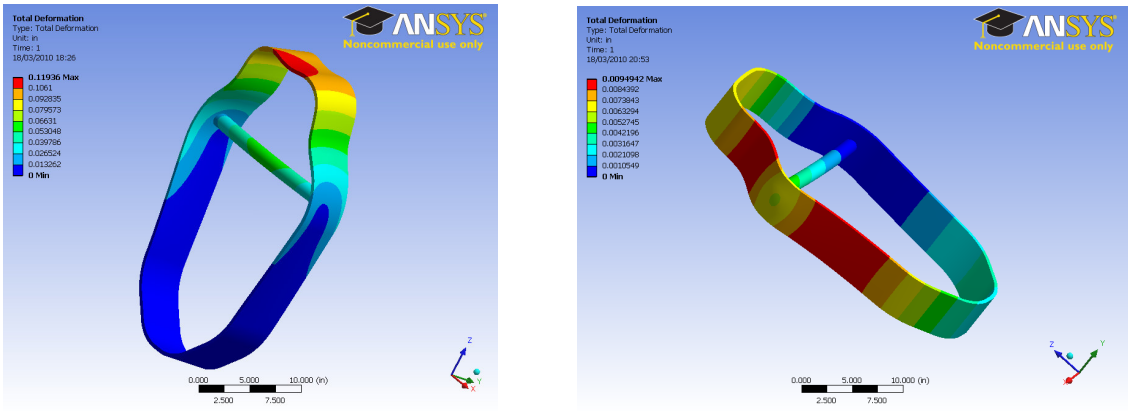

Figure 14: Roll Bar Top Load, Deflection (Left), Roll Bar Side Load, Deflection (Right)

The deflection results from hand calculations and FEA are very close to each other and also close to the testing results (see Section 4.8) once the fixturing foam is taken into account. All three results show that the roll bar passes the requirements in the ASME HPVC 2010 Rules.

4 Testing

The team performed tests in three key areas: aerodynamics, mechanics, and materials. For the aerodynamics, the range of motion for several riders was determined in order to shape the fairing around them, two new methods were tested to determine the C_d of a human powered vehicle, and tuft testing was performed to evaluate flow characteristics on a full scale model. For vehicle mechanics, different chain ring shapes and crank lengths were tested in order to determine the combination that maximizes the power output. Also, tests were performed to determine the most stable configuration of the tilting trike mechanism. For materials, tests were performed to compare several possible construction materials in order to select the best materials for the application. In addition, destructive testing of a mock up of the roll bar was performed to ensure that it met the ASME HPVC safety specifications.

4.1 Stability Testing

After the basic configuration of the tilting trike was determined, the major parameters were varied to determine the most stable configuration. Initially the angle of the vehicle frame with respect to the ground was defined as the stability criterion, with the reasoning that a perfectly stable vehicle would always be 90° from the ground and an unstable vehicle would lean towards the ground and require correction by the rider. However, once a system to measure this angle was implemented on the prototype and preliminary testing was conducted, that definition was determined to be

inadequate. It was found that a rider could make constant corrections through the handlebars and keep an unstable vehicle essentially vertical. The stability criterion was therefore redefined to be the amount of deviation of the steering mechanism from the center position. This measure of stability limited testing to straight track conditions. However, experience dictated that the most important area for stability was the start of a drag race, where the track will be essentially straight.

Several parameters were identified for optimization of the stability of the vehicle: distance between the rear wheels, the truss angle, and camber of the rear wheels. These parameters are shown below in Figure 15.

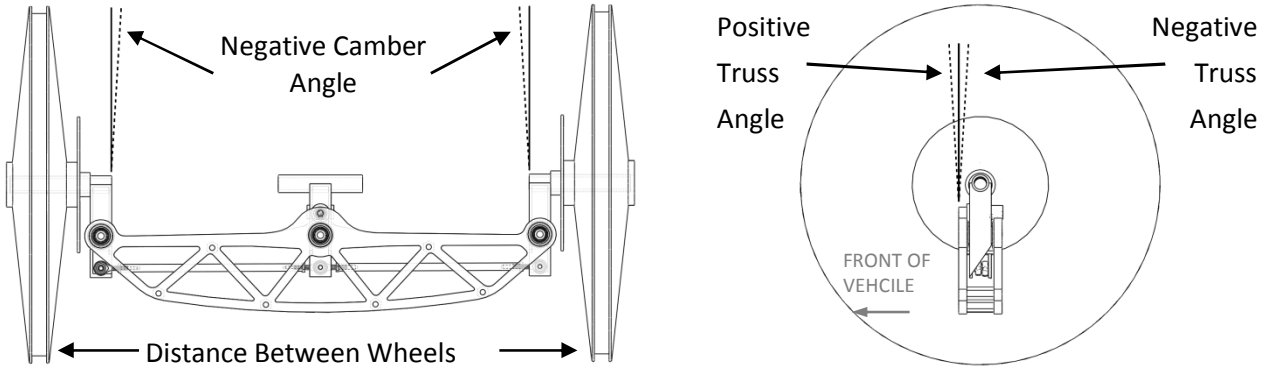

Figure 15: The Parameters Tested for Effect on Stability

The rider was timed for several runs on a 150 ft (45.7 m) track at each test configuration. The angular position of the steering mechanism was recorded using Logger Pro then exported to Excel for analysis. In order to get a metric of the stability during the entire length of the test run, the integral of the absolute value of the displacement of the steering mechanism from the center position was computed, a value labeled the "stability metric". A larger value of the stability metric would be considered more unstable because the vehicle required more steering correction.

Research indicated that any amount of camber on the wheels resulted in a significant loss of power [7]. Therefore it was decided to have zero camber on the tilting trike mechanism regardless of its effect on stability. The minimum distance between the wheels in order to clear the fairing at the desired lean angle and the maximum distance between the wheels while still receiving the maximum number of points for the width of the vehicle in the practicality section were within 1 in. (2.54 cm) of each other. Therefore it was decided that the distance between the wheels would be fixed at 26 in (66.0 cm) in order to make the outer extremes of the wheels (now the widest point of the vehicle) exactly at the required maximum distance. The truss angle was varied at the previously specified camber and distance between wheels. Levene's test confirmed the assumption of homoscedasticity, or equal variance of data among the tested truss angle positions. This assumption allows for the use of an ANOVA test to determine whether there is statistically significant difference among the tested truss angle positions. The resulting confidence intervals for the stability metric of each truss position are shown below in Figure 16. The truss angle position is proportional to but not equal to the truss angle.

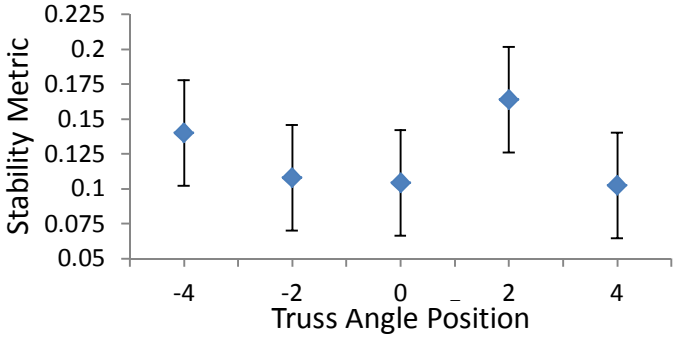

Figure 16: Stability metric sample means and confidence intervals at a 95% confidence level

The extreme values (4 and -4) were rejected because the riders were very polarized at these values; some riders performed very well while others performed very poorly. There was no statistical difference between the remaining two most stable positions (-2 and 0). To determine the best of these two positions and the intermediate position (-1), an obstacle course was assembled that included a slalom, a 180° sharp turn, and a straightaway. A single blind test was

conducted in which riders were allowed to ride two laps of the course at unknown truss angles and give opinions on how much they liked the position, how stable it felt, and how responsive the position was. This subjective data favored the -2 position. The decision was then made to set the truss angle to -1.5, which corresponds to -10.6°.

4.2 Power Chair Testing

Last year, testing was performed to find the optimal seat angle and height for the rider to sustainably deliver the maximum amount of power to the pedals. To further improve the rider's performance this year different crank lengths and chain ring geometries were tested. The tested factors are displayed in a main effects plot in Figure 17.

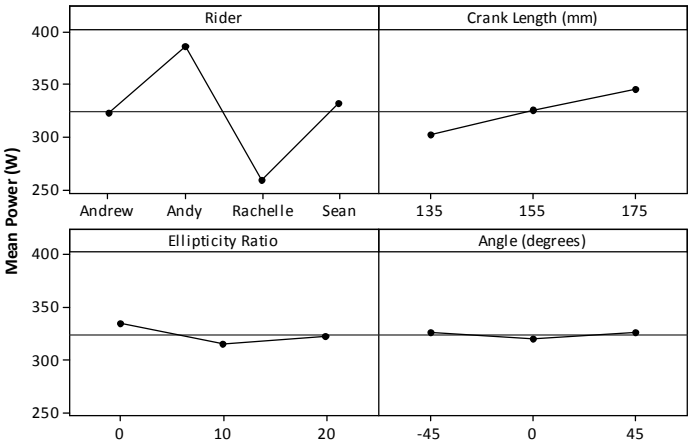

Figure 17: Main Effects Plot of Power Chair Testing

An ellipticity ratio of zero represents a traditional circular chain ring with increasing value indicating a more elliptical chainring. To further investigate the effect of the elliptical chain ring, the orientation of the cranks with respect to the chain rings greatest diameter was varied. Crank orientation was determined to be an insignificant factor. Also, the circular chain ring had the largest mean power output, so circular chain rings will be used on the Ragnarök. In general, circular chain rings are the preferred design choice because they are commercially available and create less irregularity in chain tension on the slack side of the drive train.

Crank length and rider were both shown to be significant factors during testing. In general, the riders performed better with the larger, 175 mm crank length. This trend is shown in Figure 18.

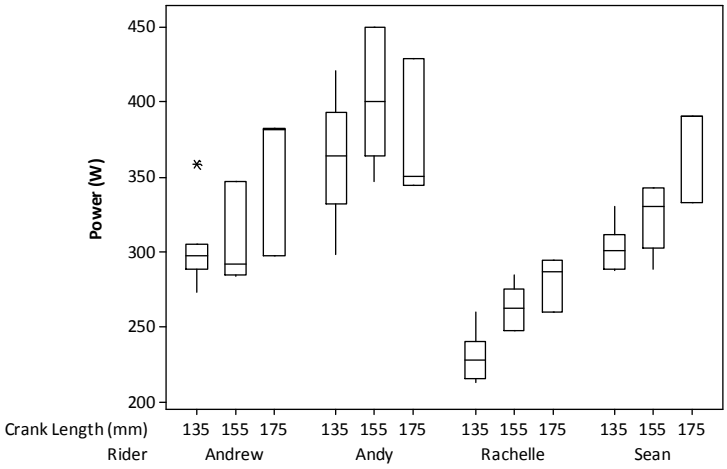

Figure 18: Interquartile Boxplots of Rider Performance with each Crank Length (the Asterisk is an Outlier)

While the testing indicates that the maximum power output occurs when 175 mm crank length is used, fitting cranks of that size inside the fairing of the Ragnarök would result in a less aerodynamic shape. Also, the riders nearly unanimously preferred the 155 mm crank length. As a result a compromise has been made to select 155 mm as the crank length for the Ragnarök.

4.3 3-Dimensional Motion Capture Testing

Motion capture testing was conducted to improve the accuracy of the internal vehicle dimensions. Test subjects rode a recumbent trainer built to dimensions consistent with the results of power output testing conducted last year. Data was

collected from each rider as they started to pedal, maintained a comfortable endurance pace, and finally sprinted. Three IR cameras controlled by Qualisys Track Manager recorded the three-dimensional location of reflective balls worn on the joints of each rider.

This testing fully captured the posture and motion of the rider. Prior designs, based on body measurements, could not accurately account for the bending of the spine and position of the head. Such models also treated the ankle as a fixed joint, while testing shows flexing at the ankle produces deviations of up to 1 in (25.4 mm) from the expected path of the heel. Motion capture testing also facilitated quantification of lateral movement of the upper body such as might be used to maintain balance, which was in the range of 0.87–1.10 in (22–28 mm) at the shoulders for different riders.

4.4 Wind Tunnel Testing

In the past, the Rose-Hulman HPVT has primarily relied on the results of FloWorks simulations to determine the drag coefficient (C_d) and flow paths of the designed vehicle for the purposes of aerodynamic refinement. This year, the team performed several tests in a wind tunnel in order to validate the results from the CFD simulations. The full report on this testing can be found on the Rose-Hulman HPVT website here: http://www.rose-hulman.edu/hpv/2010-downloads/. The drag force was measured on a scale model of the 2009 vehicle, the Mark IV, using a sting balance and Particle Image Velocimetry (PIV) and compared to the values generated using CFD. These two methods were also evaluated as possible alternatives to CFD analysis in order to obtain the C_d for a particular design. A scale model of the 2010 vehicle, the Ragnarök, will be constructed and tested for additional comparison and the results will be presented during the design presentation at the competition.

Before the testing could begin, a model of the Mark IV had to be constructed. A scale of 1:10 was chosen to reduce the wind tunnel area blockage to 4.0 % in order to prevent interference of the boundary layer from the sides of the wind tunnel. The maximum speed of the wind tunnel, approximately 150 mph (67.1 m/s), set the maximum Reynolds number of 1.0×10^6 based on model length. This scale model Reynolds number for the wind tunnel model corresponds to a full scale Reynolds number of approximately 15 mph (6.7 m/s). The full scale Reynolds number for a racing speed of 45 mph (20.1 m/s) is approximately 3.0×10^6. It is known that usually the C_d is a function of Reynolds number, however there is a region of Reynolds numbers in which the C_d is approximately constant and does not vary with the Reynolds number. This region is known as the bluff body region. Since the scale model could not be tested at the correct Reynolds number, this testing also tried to determine if the scale model Reynolds number of 1.0×10^6 was within the bluff body region which would mean that the measured C_d could be applied to the full scale vehicle at racing speed.

4.4.1 Sting Balance Testing

The scale model was mounted in the wind tunnel as shown in Figure 19 and the drag force was measured for several different tunnel speeds.

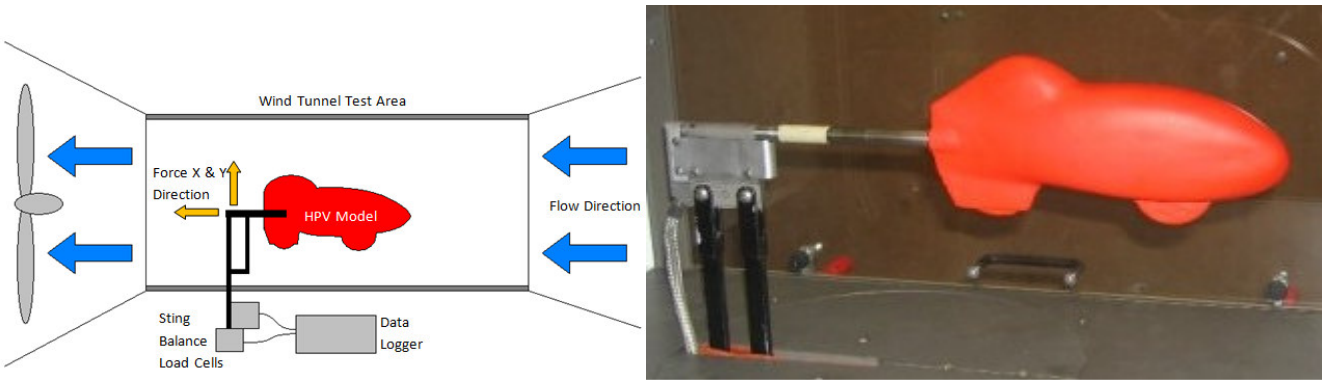

Figure 19: Sting Balance Testing Setup

Data was taken for a range of Reynolds numbers from 2.0×10^5 to 1.0×10^6 and the calculated C_d as a function of Reynolds number was plotted, as shown in Figure 20.

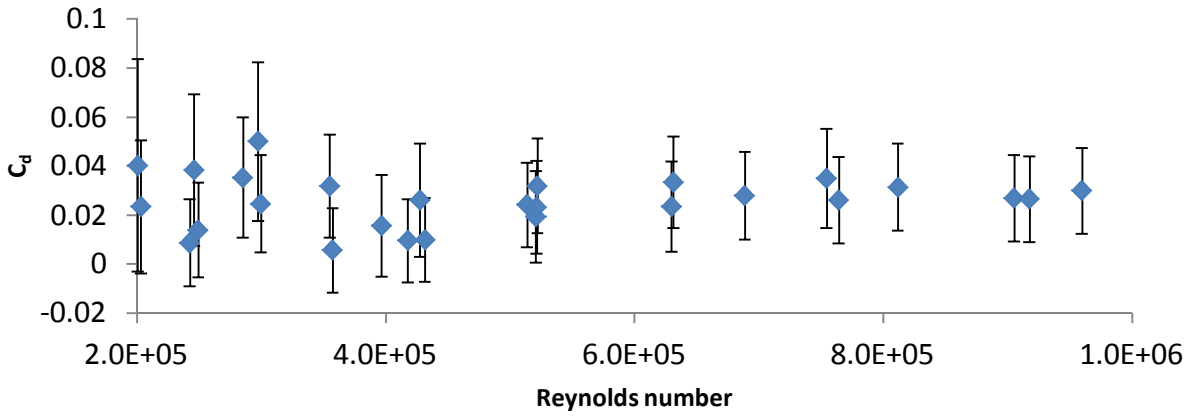

Figure 20: Variance of C_d

The vertical error bars show the uncertainty associated with each measurement. This uncertainty is a combination of the readability and accuracy of the manometer used to measure the wind speed and the accuracy and readability of the sting balance. The high error shown during tests with a Reynolds number below $5.0x10^5$ is a result of the error in readability due to fluid level fluctuations in the manometer during the tests. The average value of these readings is a C_d value of 0.03 which lies well within the error bars of all the tests with a Reynolds number greater than $5.0x10^5$ and most of the tests below. Also, the C_d appears to be constant for the testing region so the assumption that the vehicle is in the bluff body region is valid. Thus the C_d for a Reynolds number of $3.0x10^6$ can be expected to also be 0.03. The uncertainty analysis gives an uncertainty of ±0.02 for the C_d. Therefore the C_d measured using the sting balance is 0.03 ± 0.02.

4.4.2 Particle Image Velocimetry

Particle Image Velocimetry (PIV) is a testing system wherein a pulsed laser produces a laser sheet to illuminate microscopic glycerin particles suspended in the fluid flow around the body in question. While the particles are being illuminated, high speed cameras take two pictures of the particles. Then the two pictures are compared using the LaVision software to map the translation of the individual particles. This translation distance can be measured after calibration of the cameras. Since the time interval between the laser pulses is known it is possible to determine the velocity of each particle in the flow. This information is used to generate a velocity field for the fluid during the test. This velocity profile can be combined with the concept of momentum deficit to calculate the drag force then the vehicle C_d. Momentum deficit is based on conservation of linear momentum applied to a control volume consisting of the fluid surrounding the model, excluding the model itself. The resulting general equation is shown in Equation 15, where the integral terms represent the momentum of the fluid before and after encountering the vehicle.

$$0 = \frac{\delta \vec{P}_{sys}}{\delta t} = F_d + \left[\int_{A_{boundary}} \rho\left(\vec{V}_{rel} \bullet \left(-\hat{n}\right)\right)\vec{V}_{abs,x} dA \right]_{entering} - \left[\int_{A_{boundary}} \rho\left(\vec{V}_{rel} \bullet \hat{n}\right)\vec{V}_{abs,x} dA \right]_{leaving} \quad \text{Equation 15}$$

The laser is mounted above the wind tunnel, a cylindrical lens was used to fan out the laser into a sheet, and the cameras are placed to the side of the laser sheet. The testing setup is shown in Figure 21.

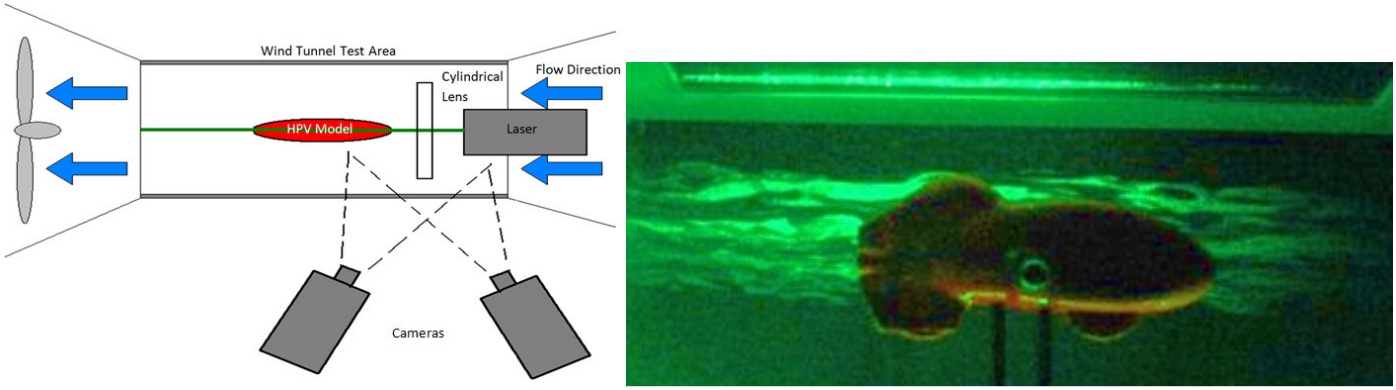

Figure 21: PIV Testing Setup: Top View Diagram (Left) and Side View Live Testing (Right)

In order to evaluate Equation 15 it was necessary to generate a profile of the velocities of the fluid perpendicular to the fluid flow both before and after the model. This was done by taking several slices parallel to the fluid flow on one half of the vehicle and using symmetry to calculate the momentum deficit for the whole vehicle. These velocity profiles, in numeric values for magnitude in each of the principal directions, were exported into MATLAB. In MATLAB the sections before and after the model for each laser sheet were spliced to a velocity profile before and after the vehicle which was perpendicular to the flow instead of parallel. Each perpendicular velocity profile was integrated numerically then substituted into Equation 15 in order to get the drag force and by extension the C_d. The result is that a C_d was calculated to be 0.141.

This testing method is less than ideal because it required moving the laser, refocusing the camera, and refocusing the Scheinflug filter on the camera for each new laser plane so that the whole of the laser plane is in focus rather than a small portion. Each refocusing also required a calibration which introduces error.

4.4.3 Results and Conclusions

The results from both the PIV and the sting balance testing are shown in Table 10 in addition to the value of the C_d determined using CFD. The uncertainty on the CFD and PIV C_d values is not known. The table also shows the theoretical max speed assuming all other effects, such as rolling resistance and wheel hole drag, are negligible and a rider power output of 350 W.

Table 10: Wind Tunnel Testing Results

	Drag Coefficient	Reynolds Number	Max Speed
Sting Balance	0.03 ±0.02	$7x10^5$-$1x10^6$	85 mph
PIV System	0.141	$1x10^6$	51 mph
CFD	0.0789	$3x10^6$	62 mph

While the results are significantly different from each other, prior art suggests that a C_d in the range of 0.02 and 0.12 is acceptable for fully faired human powered vehicles so the values are not entirely inaccurate [8,9,10]. The theoretical max speed for each C_d is unreasonably high, except from the PIV testing, which shows that there are other factors not modeled in this testing which affect the maximum speed of the vehicle.

The significant cost, in both money and time, associated with iterative testing in a wind tunnel make both the PIV and sting balance testing impractical for the large number of iterations required to fully develop a human powered vehicle fairing. Another source of inaccuracy is in the surface finish of the model when compared to the surface finish of the full scale vehicle. The wind tunnel model has a much lower surface roughness which can significantly reduce the measured drag when compared with that experienced during a human powered vehicle race. Since CFD is such an economical and relatively easy alternative to wind tunnel testing, the Rose-Hulman HPVT will continue to mainly use CFD for aerodynamic analysis and fairing refinement.

4.5 Tuft Testing

A tuft test is a full scale test that gives insight into the flow of air around a vehicle. Tufts of yarn or another light material are attached to the outside of the vehicle or a replica. The motion of the tufts in the presence of air flow can reveal

areas of laminar and turbulent flow, vortices, approximate streamlines, and stagnant air layers that result from flow separating from the vehicle. Videos of this testing are available here: http://www.rose-hulman.edu/hpv/2010-downloads/.

The male mold, which exactly matches the shape of the Ragnarök's fairing, was used in the experiment. The mold was mounted at a distance from a vehicle that carried it so that the mold would travel through undisturbed air. The motion of the tufts of yarn was captured with video and high-resolution still images. Data was taken at 10, 20, 30, 40, and 50 mph (4.5, 8.9, 13.4, 17.9, and 22.4 m/s). The first round of testing revealed much tuft motion near the rear of the vehicle. To investigate further, tuft density was increased in this area and more data was collected. The motion among the tufts near the rear of the vehicle is indicative of a transition to turbulent flow. Observations suggest that flow is laminar at most points on the mold until 64 in (1.6 m) from the nose. Also, flow separation at the rear of the head bubble is evidenced from the motionless, hanging tufts in this area, as shown in Figure 22.

Figure 22: Separated Flow (Left) and Attached Flow with Vortex Generators (Right)

Flow separation creates an area of low-pressure air at the rear of the vehicle, which increases pressure drag. In an attempt to counter this effect, Vortex Generators (VGs) were placed on the mold ahead of the separation region where the flow was still attached. VGs are commonly found on airplane wings and racecars. The fins on a VG act as wings, creating opposing areas of high and low pressure. The high pressure air will roll over the top of the fin, creating a vortex. These vortices will delay separation of the air layer flowing over airfoils by increasing the flow's momentum. Two different VGs fabricated for the Ragnarök and an illustration of their operation are shown in Figure 23.

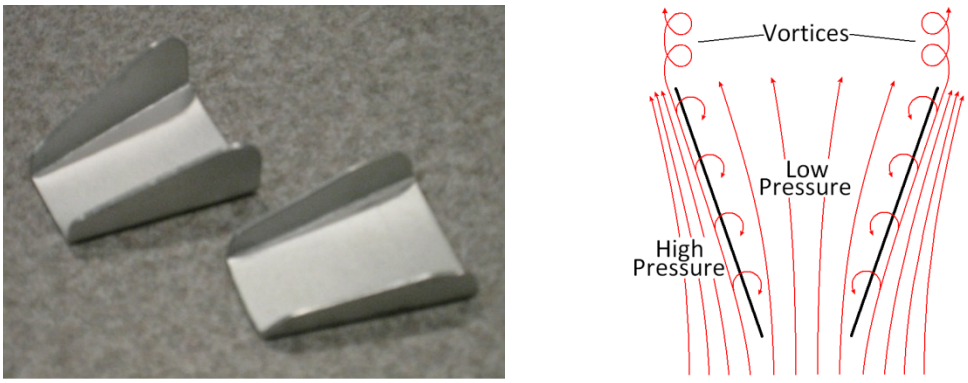

Figure 23: Vortex Generators (left), Operating Principle Diagram (right).

VGs are typically placed at the thickest point of airfoils, suggesting that they should be placed at the widest point on the Ragnarök. This point occurs approximately 5 ft (1.5 m) from the nose. The important dimension of the VGs is the height of the fins. If the fins are too low, maximum effect will not be achieved. Exceedingly tall fins will increase drag on the VG itself while not further reducing pressure drag on the vehicle. In a study by Mitsubishi Motors the optimum height of VG fins is found to be approximately equal to the thickness of the boundary layer of the flow over the vehicle at the point they are located [11]. The thickness of the boundary layer over a flat plate for laminar and turbulent flow is given by Equation 16 and Equation 17, where δ is the boundary layer thickness, x is the distance from the leading edge of the plate, and Re_x is the Reynolds number evaluated at x.

$$\delta = \frac{4.91x}{Re_x^{\frac{1}{2}}} \quad \text{Equation 16}$$

$$\delta = \frac{0.38x}{Re_x^{1/5}} \quad \text{Equation 17}$$

A δ value of 0.20 in (0.5 cm) was found for entirely laminar flow and 1.25 in (3.1 cm) for entirely turbulent flow. If the flow transitions from laminar to turbulent before the point at which the VGs are located, then an intermediate value for δ will be present. To account for the possibility of early turbulence and to ensure full effect is achieved; VGs with 0.28 in (0.7 cm) tall fins were fabricated and placed on the mold for tuft testing. Another set of VGs, with fins 0.5 in (1.3 cm) tall, was also tested. The results for the 0.5 in (1.3 cm) tall VGs were favorable, as can be seen in 4.5.

Tufts that were previously motionless are now aligned with the flow. This indicates that the flow of air is staying attached to the vehicle which will reduce pressure drag. The 0.28 in (0.7 cm) tall VGs had a lesser effect. The other dimensions and the locations of VGs can be optimized with extensive testing, but the success of the initial VGs did not make further refinement necessary.

4.6 Skid Testing

It is certain that the Ragnarök will be pushed to the limits by its riders, and inevitably it will fall and slide on the pavement. In order to provide the maximum safety and to ensure durability after crashes; the skin (outer fairing material) of the Ragnarök needs to be able to withstand as much abrasion as possible without wearing through. A skid test was used to determine which possible skin material would be best suited to protect the rider and longevity of the vehicle.

This test was originally performed in 2008 by the Rose-Hulman HPVT [12]. The results indicated that the best material for this purpose is a hybrid carbon/Kevlar cloth with the Kevlar weave in the direction of travel. This test was performed again for the Ragnarök, but this time two different weights of ballistics grade Zylon were also tested. The materials tested were as follows: 5 osy (169.5 gsm) Kevlar control, Hybrid Carbon/Kevlar (carbon parallel to the direction of travel), Hybrid Kevlar/Carbon (Kevlar parallel to the direction of travel), 4 osy (135.6 gsm) Zylon, and 6 osy (203.4 gsm) Zylon. Test samples were made of two layers of material; an inner structural layer of carbon fiber to give the samples strength and stiffness, and an outer skin layer which was abraded against the ground during the test. The 12 x 12 in (30 x 30 cm) samples were vacuum bagged using the same manufacturing process that was used in fabricating the Ragnarök.

To test these samples a testing rig was fabricated that could hold the sample and apply 0.76 psi (5.24 KPa) between the skin and the asphalt. This was calculated to be the average pressure the skin of the Ragnarök will experience during a crash. The average weight of the vehicle and rider was divided by the contact area with the ground. The sample and rig were accelerated to 30 mph (13.4 m/s) and the sample was released so that its initial orientation was with the fibers in the direction of travel. The distance the sample traveled before coming to a stop and the amount of abrasion damage was then recorded.

In order to quantitatively compare the 5 different samples a scoring metric was established. The skid damage of each sample was inspected and 1 point was added to a sample's score for noticeable fabric fuzzing in an area (circled in blue) and 1 to 4 points were added for each area where the skin sample wore through to the carbon supporting layer (circled in red) depending on severity. The skid distances of each sample were also recorded and listed in Table 11. Figure 24 shows the wear on the skid test samples.

Table 11: Skid Testing Data and Scoring

Material Name	Kevlar	Hybrid (carbon direction)	Hybrid (Kevlar direction)	Zylon 4 osy (135.6 gsm)	Zylon 6 osy (203.4 gsm)
Abrasion Score	11	6	5	13	7
Abrasion Place	4th	2nd	1st	5th	3rd
Stopping Distance ft, in (m)	119'8" (36.5 m)	101'8" (31.0 m)	109'7" (33.4 m)	89'3" (27.2 m)	93'0" (28.4 m)
Stopping place	5th	3rd	4th	1st	2nd
Total Score	4.25	2.25	1.75	4	2.75

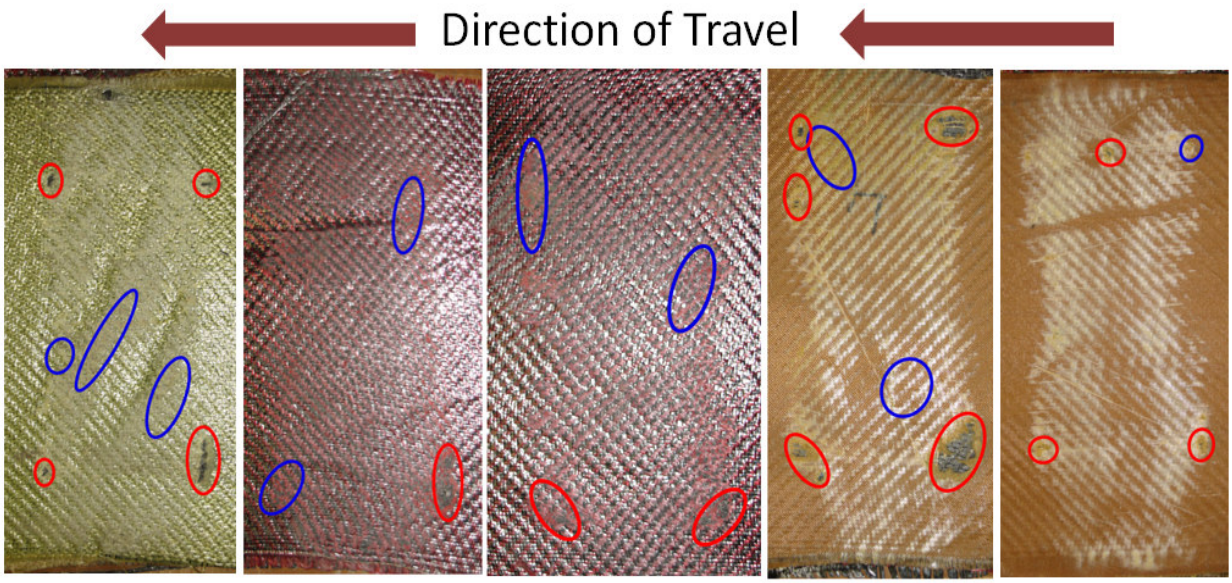

Figure 24: Samples Left to Right: Kevlar, Hybrid Carbon Dir., Hybrid Kevlar Dir., 4osy (135.6 gsm) Zylon, 6osy (203.4 gsm) Zylon

When comparing the results of the samples tested it is important to compare the amount of wear as well as the stopping distance. A low stopping distance is desired because the quicker the Ragnarök stops in a crash the less likely it is to collide with any obstacles on or near the road. The total score was calculated by using a weight of 0.75 multiplied by the abrasion place and a weight of 0.25 multiplied by the skid distance placement. It is definitely important that the Ragnarök stop quickly in a crash, but it is significantly more important to the team that the Ragnarök remain in operating condition; hence the higher abrasion weight. The sample which scored the best was the hybrid carbon/Kevlar (released in the direction of the Kevlar fibers). The second place sample was the other hybrid configuration. These tests conclusively show that the hybrid cloth in the Kevlar direction is the best choice for the skin material of the Ragnarök, confirming our previous results from 2008.

4.7 Carbon Shard Testing

In 2009 the HPVT conclusively determined the increase in safety of a Kevlar lined carbon fiber fairing when compared to a conventional carbon only fairing [**13**]. In the event of a collision the soft and net-like properties of the Kevlar will stop the razor-like carbon shards from breaking through and injuring the rider. This year the goal was to perform this test again comparing 4 osy (136 gsm) and 6 osy (203 gsm) ballistics grade Zylon to a carbon control and Kevlar samples. Four, 4 x 10 in (10.2 x 25.4 cm) samples were made for this test. Each sample had three layers of 19.7osy (668 gsm), 2x2 twill carbon cloth covered with one layer of the test material. The materials to be tested were a 19.7osy (668 gsm) carbon fabric control, a 5 osy (170 gsm) Kevlar with a 4 harness satin weave, a 4 osy (136 gsm) Zylon plain weave, and a 6 osy (203 gsm) Zylon plain weave. The samples were laid up in a medium cure room temperature epoxy and vacuumed bagged to emulate the actual vehicle fairing.

To simulate the worst crash situation possible, the samples were broken over a square edge. Due to the qualitative nature of these tests, visual inspection is the primary judge of material success or failure. A description and a score of 1-10 are given to the sample to indicate the severity of the shards and the danger to the rider. A score of 10 indicates a very safe break and a score of 1 indicates a razor-like edge.

The carbon control samples produced a significant amount of carbon shards and protruding fragments (left image, Figure 25). The orange ovals signify areas with sharp carbon fiber spikes jutting out. The yellow circles signify areas where the carbon has become discontinuous and there is a flat carbon edge exposed. Because of the significant amount of sharp carbon exposed edges and protruding shards, the carbon control samples get a safety score of 2. The 5 osy (170 gsm) Kevlar weave showed significantly less exposed carbon (yellow circles in right image, Figure 25) and no carbon fibers protruding from the surface. This level of protection warranted a safety rating of 6 for the 5 osy (170 gsm) weave.

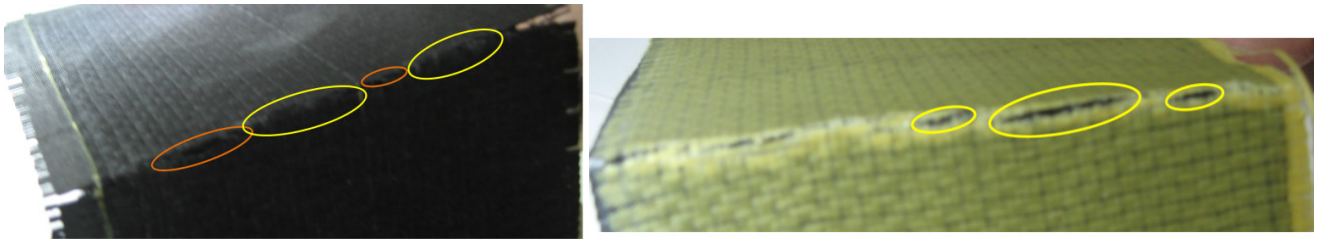

Figure 25: Carbon Control and Kevlar break through samples

Both Zylon samples exhibited significant improvements over the Kevlar and carbon control samples. Neither Zylon sample tore through at all, which, by the scoring criteria used on the first two samples, would yield a perfect score for both. However, perfect scores were not given because there was a delamination failure mode present that was not seen in the Kevlar sample. Though the carbon and Zylon were laid at the same time, the Zylon weave peeled off of the carbon as opposed to the carbon tearing through. The delaminating region (shown as area between red dotted line and solid red line in both images, Figure 26) is more than double the area in the 4 osy (136 gsm) Zylon sample (left image, Figure 26) as it is in the 6 osy (203 gsm) Zylon sample (right image, Figure 26). Because of the larger delamination area of the 4 osy (136 gsm) Zylon sample the 4 osy (136 gsm) Zylon received a safety rating of 8 and the 6 osy (203 gsm) Zylon received a safety rating of 9.

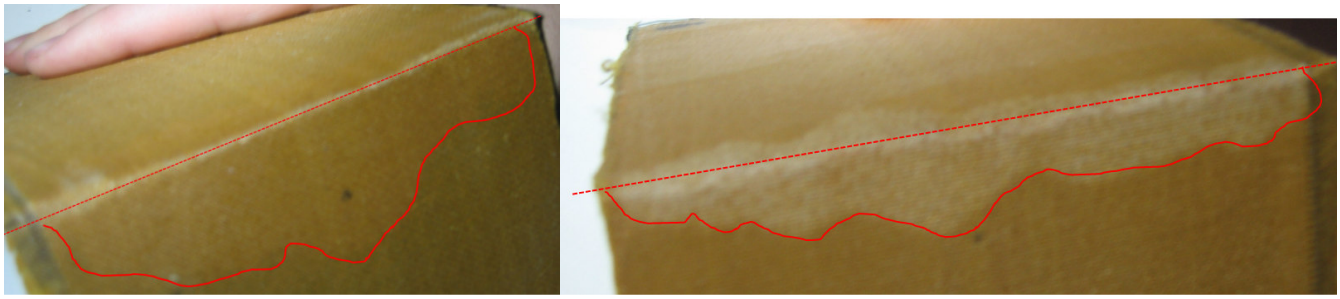

Figure 26: 4 osy (136 gsm) and 6 osy (203 gsm) Zylon crack through samples

The newly tested Zylon material greatly outperformed the Kevlar material used in the past because of its unique feature to delaminate before it is sliced through by the carbon. This property is ideal for the team's rider protection goals, and it was decided to use 6 osy (203 gsm) Zylon to line the inside of the vehicle because it received the highest safety rating and because it has a less severe delamination problem.

4.8 Roll Bar Testing

Part of the Ragnarök's rollover protection system is an integrated, composite roll bar. The roll bar was designed to encompass the tallest point on the vehicle fairing to protect the rider's head during a rollover or collision. To ensure the roll bar will be strong enough to protect the rider during collisions, a mock roll bar was tested in a tensile test machine per the specifications given in the 2010 HPVC rules. The roll bar was subjected to the 600 lb_f (2.67 kN) top load at a 12° rearward angle with a deflection of 0.76 in (1.9 cm). Most of this deflection was observed to occur in a 0.75 in (1.9 cm) thick piece of foam used for fixturing. No audible or visible signs of damage were observed during or after the test. The roll bar was then subjected to the 300 lb_f (1.33 kN) side load, experiencing a deflection of only 0.95 in (2.4 cm), which again was largely observed in the foam used for fixturing. The roll bar still appeared undamaged. The mock roll bar passed both of the required loading tests, with minimal deflection observed in the roll bar itself.

After successfully completing the specified tests, the roll bar was loaded again to determine loading at the deflection constraints. When loaded from the top, the roll bar withstood a maximum force of 1430 lb_f (6.34 kN) with a deflection of 1.42 in (3.6 cm). No foam was present for this test. To test the effectiveness of the carbon cross-tube included in the roll bar's design, the roll bar was tested to failure in the side-loading condition in a subsequent test. The roll bar withstood a maximum force of 2330 lb_f (10.4 kN) at a deflection of 3.00 in (7.62 cm). For this test, two pieces of 0.75 in (1.9 cm) foam were used in fixturing. The pieces of foam appeared to be almost entirely compressed, placing the deflection in the roll bar itself near the specified limit of 1.5 in (3.81 cm).

Videos of roll bar tests are available at http://www.rose-hulman.edu/hpv/2010-downloads/

5 Practicality

The intended end use of the Ragnarök is fast, efficient, single person transport with small amounts of cargo, requiring speed and functionality in a variety of conditions. The tilting trike mechanism allows for high speed turns and can be locked for stability in low-speed environments. The Ragnarök is primarily composed of composite materials and aluminum, both of which are well known for corrosion resistance. Also, common corrosion protection measures such a painting and anodizing have been taken to reduce the amount of exposed metals. The components used on the Ragnarök are high-end components from common bicycle manufacturers, ensuring durability and familiar operation. Maintenance free, double sealed bearings were chosen for the tilting trike mechanism so that the only maintenance required for the Ragnarök would be tasks common to upright bicycles, and standard cycling tools could be used. The front wheel and tilting trike mechanism are easily removable allowing the vehicle to be easily disassembled for transport. Experience in the recumbent cycling community shows that many who commute with recumbents also participate in races, such as those sponsored by Human-Powered Race America. To allow the end user to compete in these races with the Ragnarök, it also has to be adaptable. Such was the motivation for having the tilting trike mechanism be replaceable with a single wheel.

5.1 Conditions

The temperatures at which the Ragnarök is rideable depend on the temperature inside the vehicle. The temperature inside must remain between 41°F (5°C) and 95°F (35°C). Riding with the top fairing on, in addition to cold weather gear, helps insulate the rider from the cold. The vehicle prototype has been tested with snow and sleet on the ground with minimal effect on the performance. The trike design significantly reduces problems caused by ice because there are three points of contact with the ground. This was proven through extensive testing in both snow and ice on the prototype of the Ragnarök, see Figure 1. Since the fairing is water resistant, rain will not be a significant problem. This means that the Ragnarök should be rideable more than 320 days per year. It is possible to ride with the top of the fairing removed, allowing air flow to the rider. Therefore, it is possible to ride with ambient temperature of 30°F (0°C) all the way to 95°F (35°C) and a variety of precipitation conditions.

Using the Köppen climate classification, several regions were identified as areas where the vehicle can be ridden for most of the year. The classifications of ‘Dfa’ and ‘Dfb’, which include northern and eastern portions of the United States, have an appropriate temperature range [**14**,**15**]. Rose-Hulman’s location, Terre Haute, is within the ‘Dfa’ region and has a minimum average monthly temperature of 18°F (-7.8°C) and a high of 87°F (30.5°C) in the summer. Since only January’s monthly average temperature falls outside the aforementioned range, the Ragnarök should be able to be ridden about 334 days of the year in Terre Haute, IN.

5.2 Visibility

In order to make Ragnarök as practical and safe as possible, good visibility is required. Accordingly, this year’s vehicle is designed so that the rider can comfortably see more than 180°. Additionally, mirrors were attached to the fairing, increasing the rider’s field of view to almost 320°. Due to a more upright seat angle and a more sloped front fairing a rider can see the ground 13 ft (4.0 m) in front of the vehicle which is a significant improvement over the 2009 Mark IV. This allows for easier navigation, avoidance of obstacles, and increased safety.

5.3 Utility Features

As an unrestricted class vehicle, the Ragnarök has headlights in the lower front of the vehicle making it easily visible even in rain, fog, or darkness. For enhanced visibility from the rear, the Ragnarök’s tail features a stripe of red reflective tape and red taillights while the side of the vehicle will display amber reflective tape. This is especially valuable at night or on the roadside where car headlights will make the tape stand out. The only requirements for riding after dark in Indiana are that the vehicle have a white light on the front visible from 500 ft (152 m) and a red light or red reflectors in the rear which is also visible from 500 ft (152 m); the Ragnarök has all three.

In the bicycle mode the Ragnarök’s front and rear wheels can have removable mud or splashguards. In trike mode the rear wheel hole in the fairing can be blocked with a removable cover. The Ragnarök has a loud piezzo buzzer in place of a bell in the bottom of the fairing. This buzzer can be triggered by the rider to warn others in the vicinity. This buzzer can be louder than a conventional bell and also programmed to change pitch, which can make the sound more noticeable. For theft protection, a conventional bicycle lock can be used to secure the Ragnarök to an object or prevent a rear wheel from freely rolling.

5.4 Special Features

To facilitate the commuting end user, the Ragnarök features a bladder-type water bottle that is integrated into the seat. The tube and bite-valve are routed through holding loops along the seat to a convenient location. This design utilizes a pouch to make the bladder easily removable for rapid pit stops. For longer commutes and endurance races, a rider needs electrolyte and carbohydrate replacement. Velcroed into the top are two removable pockets that are easily accessed by the rider. One pocket could contain a standard bicycle-type water bottle with these supplements in liquid form while the other pouch is generic and enables the rider access to a small storage of food or other small objects.

To further the reliability of the Ragnarök as a commuting vehicle, a bicycle repair kit including spare tubes, a chain breaker and multi-tool can be attached to the rollbar cross tube behind the rider and can be removed if desired. To inflate the tires a frame pump can also be stored behind the seat.

The commuting audience also needs turn signals to alert surrounding vehicles of the fully faired vehicle's intended actions. The Ragnarök features turn signals embedded in the tail of the vehicle. The signals themselves are a series of LED lights that are triggered by toggling pushbuttons located on the handlebars.

The design of the Ragnarök also meets the needs of hobbyists such as those who race in the HPRA sponsored events. Significantly more airflow is needed in a vehicle during these long distance events. However, this airflow through the cabin of the vehicle is detrimental to aerodynamics and not necessary for short distance sprint events. To comply with these constraints the Ragnarök has a NACA duct located directly in front of the wind shield that opens downwards into the vehicle acting as an air scoop and can be shut during speed events. Additionally, the Ragnarök is designed with its own custom speedometer and cadence display as described in section 2.4.6.

6 Safety

Safety was a major consideration in every design decision made for the Ragnarök. The ribbed tub frame fairing design was chosen partly for the greatly increased crash protection provided over a separate frame with non-structural fairing. Fairing materials were chosen for abrasion resistance and the ability to capture broken carbon shards. Because it plays a key role in crash protection, the roll cage was designed to meet and exceed all of the specifications required by the HPVC rules. Stability testing was performed to reduce the likelihood of crashes and to improve riders' ability to react and maneuver in a dangerous situation. Forward visibility was improved to allow riders to better assess hazards and headlights, taillights, and reflective tape has been used to improve the Ragnarök's visibility to other bikes or cars. An integrated hydration system and NACA duct protect the rider from heat sickness. In addition to all of these safety considerations, two additional features have been added solely to increase the overall safety of the Ragnarök, and are described below. As a result, all safety requirements for ASME and HPRA have been met.

6.1 Communication

Even with the attempts to maximize rider visibility outlined in Sections 5.2 and 5.3, there may arise situations when the rider is not aware of obstacles on the course, which can lead to unsafe situations sometimes resulting in crashes. In an attempt to minimize such occurrences, the HVPT will be using a collection of two-way radios to communicate between the team and the riders. There will be one two-way radio inside the bike. Riders will use temple transducer headsets, which allow for clear communication without blocking their ears. In the event that the radios fail, the thinner fairing design this year makes direct verbal communication more possible than previous years. Also, a whiteboard will be used to pass information to the rider without the need for verbal communication.

6.2 Rider Elbow Protection

Included in the Ragnarök's rollover protection system are composite shields that extend forward from the roll bar to protect the rider's shoulders and elbows from abrasion. These composite shields are integrated into the bottom of the vehicle to protect the rider during a skid when the vehicle is being ridden without the top. The outside of these shields is covered in the carbon Kevlar hybrid fabric that provides the best abrasion resistance to protect the rider during prolonged or repeated skids.

Appendix 1: Costs

Fabrication Consumables

Vehicle Components	$1100.81
Composite Materials	$955.11
	$2065.92 (per vehicle)

Mold Construction

Materials	$393.06
	$393.06 (per mold)

Employees

Floor Workers (10 at $15 per hour)	$26000.00
Machinists and Welders (2 at $20 per hour)	$6933.33
Engineers (5 at $38 per hour)	$32933.33
	$65,866.67 (per month)

Other Costs

Building Rental	$2500.00
Utilities	$1000.00
Advertising	$1000.00
Employee Salaries	$65866.67
	$2065.92 (per month)

Equipment

Milling Machine	$4000.00
Grinders	$400.00
Lathe	$3000.00
Welder	$2500.00
Band Saw	$1500.00
Vacuum Pumps	$1000.00
	$12,400.00

(values in dollars)	Year 1	Year 2	Year 3	Year 4	Year 5	Year 6
Machine Initial Costs	$12,400.00					
Tools	$2,000.00	$2,000.00	$2,000.00	$2,000.00	$2,000.00	$2,000.00
Maintenance			$3,000.00			$3,000.00
Vehicle Materials	$247,910.40	$247,910.40	$247,910.40	$247,910.40	$247,910.40	$247,910.40
Mold Materials	$1,179.18	$1,179.18	$1,179.18	$1,179.18	$1,179.18	$1,179.18
Other Costs	$247,910.40	$247,910.40	$247,910.40	$247,910.40	$247,910.40	$247,910.40
Vehicle Sales	($587,400.00)	($587,400.00)	($587,400.00)	($587,400.00)	($587,400.00)	($587,400.00)
Cash Flow	($76,000.02)	($88,400.02)	($85,400.02)	($88,400.02)	($88,400.02)	($85,400.02)
Period	0	1	2	3	4	5
Net Present Value	$76,000.02	$85,000.02	$78,957.12	$78,587.30	$75,564.71	$70,192.59
Total Profit (Present Value)	$464,301.75					
Interest Rate	0.04			Initial Investment	$15,579.18	
Per Vehicle Sales	$4,895.00			Also covers two month costs	$263,489.58	

References

[1] Wittingham, S., Interview by Harvey, T. Battle Mountain, NV, 9 May 2007.

[2] Roark, R., 1989, *Formulas for Stress and Strain*, 5th ed., R. R. Donnelley & Sons, Chicago, IL.

[3] National Weather Service, 2009, "Observed Weather Reports," National Oceanic and Atmospheric Administration, Silver Spring, MD, http://www.weather.gov/climate/index.php?wfo=ind.

[4] Celik, A.N., 2004, "A statistical analysis of wind power density based on the Weibull and Rayleigh models at the southern region of Turkey," Renewable Energy, **29**(4), pp. 593-604.

[5] Dorvlo, A.SS., 2002, "Estimating wind speed distribution," Energy Conversion and Management, **43**(17), pp. 2311-2318.

[6] Seguro, JV., and Lambert, TW., 2000, "Modern estimation of the parameters of the Weibull wind speed distribution for wind energy analysis," Journal of Wind Engineering and Industrial Aerodynamics, **85**(1), pp. 75-84.

[7] Kolodziejzyk, G., 2004, "Camber and suspension watts test," Adventures of Greg, , http://adventuresofgreg.com/blog/2004/10/26/camber-and-suspension-watts-test/.

[8] Beauchamp, W. Recumbents.com. 7 April 2002, http://www.recumbents.com/wisil/simul/HPV_Simul.asp

[9] Malewicki, D., 1983, "Unified Performance Graphs and Comparisons for Streamlined Human Powered Vehicles," *Second International Human Powered Vehicle Scientific Symposium: Proceedings*, International Human Powered Vehicle Association, Indianapolis, INpp. 46-59.

[10] Voigt, A., 1981, "Analysis of Aerodynamics and Mechanics of HPVs," *First Human Powered Vehicle Scientific Symposium Proceedings*, International Human Powered Vehicle Association, Indianapolis, INpp. 112-125.

[11] Koike, M. et al., 2004, "Research on Aerodynamic Drag Reduction," Mitsubishi Motors, Tokyo, http://www.mitsubishi-motors.com/corporate/about_us/technology/review/e/pdf/2004/16E_03.pdf.

[12] Rose-Hulman Institute of Technology Human Powered Vehicle Team, 2008, "2008 Rose-Hulman HPVT Design Report," Rose-Hulman Institute of Technology, Terre Haute, In, http://www.rose-hulman.edu/hpv/design-reports/2008/(RHIT,%202008)2008%20Team%2035%20Design%20Report_west%20(Rose-Hulman).pdf.

[13] Rose-Hulman Institute of Technology Human Powered Vehicle Team, 2009, "2009 Rose-Hulman HPVT Design Report," Rose-Hulman Institute of Technology, Terre Haute, IN, http://www.rose-hulman.edu/hpv/design-reports/2009/rhit-2009-singlerider.pdf.

[14] Food and Agriculture Organization of the United Nations, "Brief Guide to Koeppen Climate Classification System," Food and Agriculture Organization of the United Nations, Rome, Italy, http://www.fao.org/WAICENT/faoinfo/sustdev/EIdirect/climate/EIsp0066.htm.

[15] Pidwirny, M., 2009, *Fundamentals of Physical Geography*, 2nd ed., Irving K. Barber School of Arts and Sciences, Kelowna, BC, Chap. 7, http://www.physicalgeography.net/fundamentals/7v.html.